Second review of the paper acp-2018-1139
**« Large-eddy simulation of radiation fog with
comprehensive two-moment bulk microphysics: Impact of different aerosol activation and
condensation parameterizations»**

from Johannes Schwenkel and Björn Maronga

RC2: General comments : Significant improvements have been brought in this second version and authors have made significant efforts to address criticisms. For instance a prognostic approach of supersaturation has been added and has made a substantial contribution, allowing also to correct a bug. But there are still some weaknesses, inaccuracies and confusion, making the paper not suitable for publication in ACP. Therefore I recommend a second revision before publication.

Author's answer: First of all we would like to thank the reviewer again for the constructive and helpful comments. With this review we have shifted our main focus (what has been missed during the last revision) of this paper to the new introduced results concerning a comparison of different supersaturation calculations in a two-moment microphysics scheme. With the help of these comments, it was possible to contribute to a significant improvement in the work and to clarify paper.

My major concerns are:
RC2: - The sensitivity of the supersaturation parametrization is presented in 2 parts without a clear link between them, and the key conclusions are not clear. Indeed, a first part (4.2) refers to 1-moment microphysical scheme (as nc is fixed) and concludes to the negligible sensitivity of the supersaturation parametrization. But this test is not interested as firstly most of LESs use a 2-moment scheme, and secondly a prognostic saturation is only of interest if droplet concentration is prognostic. It would have no sense if a prognostic saturation scheme was associated with a 1-moment scheme. The second part (4.4) refers to 2-moment scheme and concludes to the importance of supersaturation parametrization as LWP is significantly changed. This 2nd test is the most interested. Additionally, these 2 parts are separated by a sensitivity test of activation parametrization
(4.3). Therefore the conclusions are confusing and the paper does not appear beautifully built. From my point of view, the best would be to remove the test of supersaturation parametrization with 1- moment scheme. But if the authors want to keep it as I suppose, it is necessary to merge those parts (with 2 subparts : 1-moment and then 2-moment scheme) and to enhance the conclusion with the 2- moment scheme. The main conclusion will be in agreement with Thouron et al. (2012) with a new aspect concerning application to radiative fog. The conclusion must be revisited too, considering this aspect.

Author's answer: We agree with that objection. We followed your advice and have restructured the paper as suggested. Moreover, we also clarified our conclusion and set the focus to the two-moment microphysics using different methods for calculating the supersaturation. However, we would like to keep the part with the one-moment microphysics scheme as it was an open question that needed to be addressed. However, we shortened this chapter and put the focus on the main result that the error can be neglected.

Modification: As this comment result in a restructuring and major modification of chapter 4 and 5 we would like to refer to the marked-up manuscript in which all modifications are highlighted.

RC2: - Concerning the supersaturation parametrization again, that would make it clearer if the method called « explicit supersaturation calculation » was replaced by « diagnostic of supersaturation » to be distinguished from the prognostic approach (as the prognostic approach is also explicit). This would require to replace EXP with DIA in all the text and figures. For the prognostic supersaturation, it is not clear if the supersaturation is advected ? If not, it would be better to call it « pseudo-prognostic » as in Thouron et al. (2012). P9, there is a confusion between d

and s used previously. What is their difference?

Author's answer: We agree with the first point, and have renamed the method, which was previously named by *'explicit supersaturation'* to *'diagnostic supersaturation'*. Therefore, all corresponding figures and text parts were adopted. The objection is correct and hence this modification may improve the comparability with other studies. Concerning the second point: Yes our supersaturation is advected and is therefore represented as an own prognostic quantity. We decided to implement this method (after consultations with a former colleague), which basically follows the implementation described in Morrison and Grabowski, 2008, (but no extra term for inhomogenous mixing). Due to that we would prefer to leave the abbreviation *'PRG'* for the prognostic calculation.

The usage of the absolute supersaturation ($d = q_v - q_s$) is necessary as it simplifies the advection of supersaturation (see Morrison and Grabowski , 2008, section 2b). However, as they mentioned it is also possible to derive a solution for s, but this would involves additional terms and is more complex.

Modification(p9): Note, that here the absolute supersaturation is taken, as using s would involve more terms and is more complex to solve (Morrison and Grabowski, 2007).

RC2: - Concerning the comparison of different activation parametrizations, I remain convinced that it is mainly reduced to a sensitivity test to the CCN concentration as the activation spectra of Fig.A1 show. As authors do not want to change this test for users' need, it is important to insist more on the CCN concentration change. Users must be warned that the choice of the activation method changes significantly the CCN concentration.

Author's answer: We agree with your objection as the choice of activation parametrization significantly change the CCN concentration. Therefore, we emphasized in the revised manuscript that the differences between the activation schemes are produced by different CCN concentrations and this part of the study can be understood as a sensitivity study of different CCN concentration. However, in our opinion, this is a relevant information from the user's perspective should be aware of the fact that different activation parameterizations lead to significantly different CCN concentrations and thus different fog structure.

Modification: [..] Using those different parameterizations resulting in different activation spectra, which are shown in Fig.2. One can see, that especially the CCN concentration is changed by using these different methods, such that this part of the study is equivalent to sensitivity study of different CCN concentration but realized by using different coexisting parameterizations. [..]

[..] This part of the study can be regarded as a sensitivity study of different CCN concentrations realized by applying different activation schemes, which is illustrated also in Fig 2. However, from a model user's perspective, such a sensitivity is of great importance as CCN concentrations are usually difficult (case studies) or even impossible (forecasting) to obtain and model results thus might highly depend on the chosen activation parameterization. [..]

[..] However, it must be mentioned that these differences are attributed to the fact that the CCN concentration is different for the investigated schemes. This part of the study can thus also be understood as a sensitivity study for different CCN concentrations realized by the usage of different activation schemes. [..]

RC2: - The conclusion needs to be revisited by replacing experiment names with physical terms, and by considering the sensitivity study to saturation scheme mainly for 2-moment schemes, which constitutes the main new result.

Author's answer: In the revised manuscript the conclusions have been rewritten and focusing now more on the main result of the two-moment microphysics scheme applying different supersaturation calculations.

Modification: As this comment involve major modifications we would kindly refer to the revised

manuscript and to the marked-up manuscript in which all modifications are highlighted.

RC2: - Also there are a lot of misspelling errors. A careful reading by a native english speaker remains necessary.

Author's answer: We are really sorry for having been too sloppy in the writing process. We tried our best to get rid of all language issues.

More specifically :

RC2: 1. p 2 l l6 : you can add a reference to the Meso-NH model : Lac et al., 2018 : Lac, C., J.-P. Chaboureau, et al., Overview of the Meso-NH model version 5.4 and its applications, Geosci. Model Dev., 11, 1929-1969, 2018.

Author's answer: Done.

Modification(p2, l16): Citation added.

RC2: 2. p 2 l 14 : « focusing on the influence of drag effect on and droplet deposition »

Modification(p2, l14):[..] but using the three-dimensionsl (3D) Large-Eddy Simulation (LES) mode, and focusing on the drag effect of vegetation on droplet deposition.

RC2: 3. p 2 l18 : Most of the 2-moment schemes used for fog consider radiative cooling as a term of the supersaturation equation. This remark is not relevant.

Author's answer: We agree in a sense that models explicitly used for fog should and will consider radiative cooling as a term of the supersaturation calculation. However, based on the publication of Boutle et al., 2018 some NWP models using or might use activation parameterizations and saturation adjustment without considering radiative cooling explicitly. Instead they assume a minimum vertical velocity updraft and therefore fail for correct number concentration for fog. Hence with this remark we wanted to state that some typical activation schemes are not appropriate (without extensions) for fog.

Modification(p2, l18): None.

RC2: 4. P 2 l 19 « in its development and mature stage »

Author's answer: Agreed.

Modification(p2, l19): Rewritten.

RC2: 5. P 2 l 28 : add Thouron et al. (2012) to Lebo et al. (2012). Therefore in the next sentence, you can shorten with : « Following these studies ... »

Author's answer: Agreed.

Modification(p2, l28): Rewritten.

RC2: 6. p 10 l 5 : do you use cyclic conditions ?

Author's answer: Yes we do use cyclic conditions at the lateral boundaries.

Modification(p10, l6): Cyclic conditions were applied at the lateral boundaries.

RC2: 7. P 11 l1-4 : not clear. Please rephrase

Author's answer: We agree, that the main message of the sentence remains unclear. At this point it should be noted that we have not conducted any further studies in which we have varied the aerosol parameters. However, this note is confusing as it was never claimed that this was the aim of the study and it was given only for parametrization. Therefore, we have decided to delete this sentence completely.

Modification(p11, l1-4): Deleted.

RC2: 8. For parts 4.2, 4.3 and 4.4 the numbering is not correct as you have only a single subpart : 4.2.1, 4.3.1, 4.4.1

Author's answer: Thank you for that objection. As a consequence of the restructuring of the result chapter this mistake is fixed. Furthermore, the part concerning the analysis of the budgets is ordered in an own subsection. Due to that chapters with only one single subpart are avoided.
Modification: Corrected and changed numbering.

RC2: 9. P 12 l 5 : « In this section ... » : necessary to add « with a 1-moment scheme in a LES »
Author's answer: Agreed and added to the revised manuscript.
Modification(p12, l5): In this section we discuss the error introduced by using saturation adjustment for simulating radiation fog with a one-moment scheme in a LES.[...]

RC2: 10. P 12 l 16 : instead of Mazoyer et al. (2017) you can add the new reference : Mazoyer et al. (2019) just accepted which is an experimental study : https://www.atmos-chem-phys-discuss.net/acp-2018-875/
Author's answer: Thank you for that suggestion. We replaced the citation with the currently accepted manuscript by Mazoyer et al.,2018. However, we used the citation as given on the web-page of Atmospheric Chemistry and Physics.
Modification(p12, l16): Mazoyer et al. (2017) $\rightarrow$ Mazoyer et al. (2019)

RC2: 11. P 13 l 4 : « drops rapidly in PRG and EXP »
Author's answer: Agreed and added to the revised manuscript.
Modification(p13, l4): Around 0600 UTC, which is shortly after sunrise, relative humidity drops rapidly in PRG and DIA as a direct consequence of direct solar heating of the surface and the near-surface air, preventing further supersaturation at these heights

RC2: 12. P 13 l 9 : I do not understand why differences of RH at 2m between SAT and (PRG,EXP) do not lead to differences on dissipation time at the ground.
Author's answer: This can be attributed to the different methods calculating and allowing supersaturation and liquid water in subsaturated areas. Using the diagnostic and prognostic method, liquid water can also be present in regions where the air is slightly subsaturated. In contrast, using saturation adjustment means the relative humidity is kept to saturation as long as no liquid water is present anymore. A closer look to Figure 3 shows that the times when all schemes reaches a lower relative humidity (Rh<99.8) occurs for all cases simultaneously.
Modification(p13, l9): None.

RC2: 13. Figure 5 is not nice and subfigures on the right are too small. Is it necessary to present the 3 hours for the right part with the budget ? Only 6 UTC would be sufficient as in Fig. 9.
Author's answer: As the main focus of our paper has shifted, we decided to remove this figure completely as it does not provide substantial information supporting the main objective of this paper anymore.
Modification(Figure 5): Removed.

RC2: 14. P 14 l 7 : « mature phase before sunrise, and mature phase after sunrise »
Author's answer: We agree to this. However, this part was removed from the revised manuscript.
Modification(p14, l7): None.

RC2: 15. P 14 l 9 : you cannot say that the differences between the runs are negligible as budgets discriminate 2 sets : SAT and (EXP,PRG)
Author's answer: Your objection is correct. However, for improving the clarity and pushing the focus more on the results regarding different supersaturation calculations in a 2-moment microphysics we decided to remove this part from the manuscript as it is not an essential result.
Modification(p14,l9): Deleted.

RC2:16. p 15 l 13 : « differences for activation in a 2-moment scheme might be crucial » : that is why explanations are confusing and parts 4.2 and 4.4 must be merged.
Author's answer: Agree, and changed accordingly.
Modification(p15,l13): Merged**.**

RC2:17. P 16 l 15 : this result is not new. As a minimum add a reference as Boutle et al. (2018) .
Author's answer: That is correct. We have added the missing reference.
Modification(p16,l15): A linear relationship between LWP and n_c can be found: a higher n_c leads to higher LWP, which is in agreement to other studies as e.g. Boutle et al. (2018).

RC2:18. p 17 l 1 : where are the observed values ?
Author's answer: They are added in the revised manuscript.
Modification(Fig 11): In Fig.11 the simulated visibility for the cases N1DIA-N3DIA in 2m height together with the observed values at Cabauw (for illustration only).

RC2:19. P 18 l 2 : « N2EXP suffers the most ... » : it is a negative assessment, but what is the reference?
Author's answer: Definitively "suffers" was the wrong term to describe the finding. Since there is no correct or false within this relative comparison, we decided to refrain from such assessments. Therefore, the sentence was rephrased.
Modification(p18, l2): Therefore, case N2EXP experiences the strongest loss of liquid water due to sedimentation (in relative terms).

RC2:20. P 18 l 12 : where do you show temporal evolution of supersaturation?
Author's answer: The evolution of the supersaturation is not explicitly shown in this chapter. But it is similar to the one showed in Fig. 3. However, we attached profiles of the supersaturation of 0400 UTC, 0600UTC and 0800UTC to prove our statement. Nevertheless, we would prefer not to include them within the paper, trying to avoid more figures.
Modification(p18,l12): None.

RC2:21. Part 4.4.1 : Is it the same time step for the coarser resolutions ? Otherwise the differences could be due to the impact of the time step instead of the impact of the resolution. If it is the same time step, it is necessary to specify it. If not, you have to run the coarser grids with the same time step (which will not cause instability problems).
Author's answer: Yes, we adopted the time step for the coarser simulations similar to the high resolved simulation, i.e. that simulations with 2m and 4m have a prescribed time step of 0.125s which is the minimum in the high resolved cases. Therefore, we have adopted the manuscript accordingly.
Modification(Part 4.4.1): For isolating the effect of the grid spacing, all simulations with a coarser grid spacing were carried out with the same time step of 0.125s, which corresponds to the average time step of the simulations at highest grid spacing of 1m. In this way, effects of different time steps induced by different grid spacings, could be eliminated.

RC2:22. P 20 l 19, P22 l 2 and P 23 l 1 : « microphysical parametrizations » is too vague and must be replaced by « supersaturation calculation »
Author's answer: We agree on this objection and have modified the revised manuscript accordingly.
Modification(p20,l19, p22,l2 and p23 l1): Rephrased.

RC2:23. P 21 : What's about the ratio between N2SAT and N2PRG according to the resolution?
Author's answer: We examined the differences, even though as it was not that straight forward as for the N2PRG/N2DIA as the fog life cycle differs stronger. We found that also the relative change

of N2SAT is somewhat larger by decreasing spatial resolution as the relative changes of N2PRG. More precisely, the relative differences (N2SAT/N2PRG), which are quite large anyhow, increases from 81.1% (for the 1 m case), 83.6% by using a grid spacing of 2m up to 93.2% for the case using a grid spacing of 4m in the mature phase. However, from this analysis it is difficult to say what are the reasons for that, as the fog layer is much more deeper and therefore develop differently.
Modification(p21): None.

RC2:24. In the conclusion, you have to forget abbreviations N1EXP, N2EXP ... and to explain the results in physical terms. Also when you discuss supersaturation calculation, you have to be clear between 1-moment and 2-moment microphysical scheme.
Author's answer: Thank you for that remark. We have removed all abbreviations from the conclusions. Moreover, we reviewed the whole manuscript and clarifying the conducted studies and explicitly labeled them concerning using one-moment or two-moment microphysics.
Modification(conclusion): Rewritten.

RC2:25. P 22 l 22 : add « in agreement with previous studies »
Misspelling : there are a lot of errors, the reading was not assiduous. Only a few ones are reported below.
- after a «:», you have to use a lowercase letter : in many parts of the text
- p1 l 2 : cycle
- p 3 l 8 : provides
- p 3 l 18 : startsed
- p 12 l 6 : « which differs »
- p 20 l 20 : resolutions, remove one « the », « comparison with » …
Author's answer: All reported misspelling are corrected in the revised revision. Furthermore, we have again double checked the spelling carefully.

Comment to further improvements. While rechecking the manuscript carefully, we made some additional improvements which are listed below:

- The was a double use of the variables k and A. k as a parameter for sedimentation is renamed to k_F. A as a parameter for the Activation scheme of Khvorostyanov and Curry (2006) is renamed by A_K.
- The appendix was removed as it was only one figure. Due to that the figure was placed within the manuscript which further helped to clarify the main difference between activation schemes.
- We have rephrased some sentences, as they were grammatical incorrect.
- We unified the axis label of all figure and correct them e.g. Liquid water $\rightarrow$ Liquid water mixing ratio
- The number concentration in case N2SAT in comparison with N2PRG/N2DIA was 60% higher at 0600 UTC. The value of 50% refers to the difference at 0800 UTC. This mistake is corrected in the revised revision.

Note all changes concerning the last revision are highlighted in a separate file.

Large-eddy simulation of radiation fog with comprehensive two-moment bulk microphysics: ~~Impact~~ impact of different aerosol activation and condensation parameterizations

Johannes Schwenkel[1] and Björn Maronga[1,2]

[1]Institute of Meteorology and Climatology, Leibniz University Hannover, Hannover, Germany
[2]Geophysical Institute, University of Bergen, Bergen, Norway

Correspondence to: Johannes Schwenkel (schwenkel@muk.uni-hannover.de)

Abstract. In this paper we study the influence of the cloud microphysical parameterization, namely the effect of different ~~treatment of diffusional growth~~ methods for calculating the supersaturation and aerosol activation, on the structure and life ~~cylce~~ cycle of radiation fog in large-eddy simulations. For this purpose we investigate a ~~selected~~ well-documented deep fog case as observed at Cabauw (Netherlands) using high-resolution large-eddy simulations with comprehensive bulk cloud microphysics scheme. By comparing saturation adjustment with ~~an explicit~~ a diagnostic and a prognostic method for calculating supersaturation (while neglecting the activation process) we find that, even though assumptions for saturation adjustment are violated, the expected overestimation of the liquid water mixing ratio is negligible. By additionally considering activation, however, our results indicate that saturation adjustment, due to approximating the underlying supersaturation, leads to a higher droplet concentration and hence significantly higher liquid water content in the fog layer, while ~~explicit~~ diagnostic and prognostic methods yield comparable results. Furthermore, the effect of different droplet number concentrations is investigated, induced by using different common activation schemes. We find, in line with previous studies, a positive feedback between the droplet number concentration (as a consequence of the applied activation schemes) and strength of the fog layer (defined by its vertical extent and amount of liquid water). Furthermore, we perform an explicit analysis of the budgets of condensation, evaporation, sedimentation and advection in order to assess ~~which processes have the largest spatial influence on the development of the fog layer in its different~~ the height-dependent contribution of the individual processes on the development phases.

1 Introduction

The prediction of fog is an important part of the estimation of hazards and efficiency in traffic and economy (Bergot, 2013). The annual damage caused by fog events is estimated to be the same as the amount caused by winter storms (Gultepe et al., 2009). Despite improvements in numerical weather prediction (NWP) models, the quality of fog forecasts is still unsatisfactory. The explanation for this is obvious: fog is a meteorological phenomenon influenced by a multitude of complex physical processes. Namely, these processes are radiation, ~~turbulence~~turbulent mixing, atmosphere-surface interactions, and cloud microphysics (hereafter referred to as microphysics), and which interact on different scales (e.g. Gultepe et al., 2007; Haeffelin et al., 2010).

1

The key issue for improving fog prediction in NWP models is to resolve the relevant processes and scales explicitly, or - if that is not possible - to parameterize them in an appropriate way.

In recent years ~~various studies have~~, various studies focused on the influence of microphysics on fog. In particular, the activation of aerosols (hereafter simply referred to as activation), which determines how many aerosols at a certain supersaturation get activated and hence can grow into cloud drops, is a key process and thus of special interest (e.g. Bott, 1991; Hammer et al., 2014; Boutle et al., 2018).

Stolaki et al. (2015) investigated and compared the influence of aerosols on the life cycle of a radiation fog event while using the one-dimensional (1D) mode of the MESO-NH model with a two-moment warm microphysics scheme after Geoffroy et al. (2008) and Khairoutdinov and Kogan (2000), and included an activation parameterization after Cohard et al. (1998). In other fog studies, using single-column models, different activation schemes such as the simple Twomey-power law activation in Bott and Trautmann (2002) and the scheme of Abdul-Razzak and Ghan (2000) (see Zhang et al., 2014) were applied. Furthermore, also more advanced methods such as sectional models have been used for an appropriate activation representation. Maalick et al. (2016) used the Sectional Aerosol module for Large Scale Applications (SALSA) (Kokkola et al., 2008) in two-dimensional (2D) studies for a size-resolved activation. Mazoyer et al. (2017) conducted, similar to Stolaki et al. (2015) ~~simulation of the ParisFog~~, simulations for the ParisFog Experiment with the MESO-NH ~~model~~ (for more information to the MESO-NH model, see Lac et al., 2018) model, but using the ~~3D Large-Eddy~~ three-dimensionsl (3D) Large-Eddy Simulation (LES) mode, and focusing on the ~~influence of drag effect~~ drag effect of vegetation on droplet deposition. For the fog microphysics they ~~also used an~~ used the activation parameterizations after Cohard et al. (2000) in connection with saturation adjustment. ~~This large number of~~ As outlines above, several different activation parameterizations have been employed for simulating radiation fog. This raises the question how different methods affect the structure and life cycle of radiation fog. Furthermore, schemes that parameterize activation based on updrafts (typically done in NWP models) might fail for fog. Such schemes derive supersaturation as a function of vertical velocity, which is valid for convective clouds that are forced by surface heating, but not for radiation fog, which is mainly driven by longwave radiative cooling in its development and mature phase (Maronga and Bosveld, 2017; Boutle et al., 2018).

Although great progress has been made to understand different microphysical processes in radiation fog based on numerical experiments, turbulence as a key process has been either fully parameterized (single-column models) or oversimplified (~~two-dimensional~~ 2D LES). Since turbulence is a fundamentally ~~three-dimensional~~ 3D process, the full complexity of all relevant mechanisms can only be reproduced with ~~three-dimensional~~ 3D LESs (Nakanishi, 2000).

Moreover, a disadvantage of most former studies is the use of saturation adjustment, which implies that supersaturations are immediately removed within one time step. This approach is only valid when the time scale for diffusion of water vapour (~~on~~ in the order of 2-5 s) is much smaller than the model time step~~, which~~. This is the case in large scale models where time steps are on the order of 1 min~~. However,~~, but in LES of radiation fog, time steps easily go down to split seconds so that ~~this assumption~~ the assumption made for saturation adjustment is violated and might lead to excessive condensation ~~(e.g. Lebo et al., 2012) . Following Lebo et al. (2012) and Thouron et al. (2012)~~ (e.g. Lebo et al., 2012; Thouron et al., 2012). As a follow-up to these

studies, who investigated the influence of different supersaturation calculations for deep convective cloud and stratocumulus, the present work ~~considers~~ investigates the effect of saturation adjustment on radiation fog.

As Mazoyer et al. (2017) and Boutle et al. (2018) stated that both ~~,~~ LES and NWP models tend to overestimate the liquid water content and the droplet number concentration for radiation fog, the following questions are derived from these shortcomings:

(i) Is saturation adjustment appropriate as it crucially violates the assumption of equilibrium? How large is the effect of different ~~supersaturation calculations~~ methods to calculate supersaturation on diffusional growth ~~?~~ of fog droplets?

(ii) ~~What is the impact of different activation schemes on the fog life cycle for a given aerosol environment?~~

~~(iii)~~ As the number of activated fog droplets is essentially determined by the supersaturation, how large is the effect of different supersaturation modeling approaches on aerosol activation and therewith on the strength and life cycle of radiation fog (cf. Thouron et al., 2012)?

(iii) What is the impact of different activation schemes on the fog life cycle for a given aerosol environment?

In the present paper we will address the above ~~issues by employing~~ research questions by employing idealized high-resolution LESs with atmospheric conditions based on an observed typical deep fog event with continental aerosol conditions at Cabauw (Netherlands).

The paper is organized as follows: ~~Section~~ section 2 outlines the methods used, that is the LES modeling framework and the microphysics parameterizations used. Section 3 ~~provide~~ provides an overview of the simulated cases and model setup, while results are presented in section 4. Conclusions are given in section 5.

2   Methods

This section will outline the used LES model and the treatment of radiation and land-surface interactions, followed by a more detailed description of the bulk microphysics implemented in the Parellized Large-Eddy Simulation Model (PALM) and the extensions made in the scope of the present study.

2.1   LES model with embedded radiation and land surface model

In this study the LES model PALM (Maronga et al. 2015; revision 2675 and 3622) was used with additional extensions in the microphysics parameterizations. PALM has been successfully applied to simulate the stable boundary layer (BL) (e.g. during the first intercomparison of LES for stable BL, GABLS, Beare et al., 2006) as well as radiation fog (Maronga and Bosveld, 2017). The model is based on the incompressible Boussinesq-approximated Navier-Stokes equations, and prognostic equations for total water mixing ratio, potential temperature, and subgrid-scale turbulence kinetic energy. PALM is discretized in space using finite differences on a Cartesian grid. For the ~~non resolved~~ non-resolved eddies a 1.5-order flux-gradient subgrid closure scheme after Deardorff (1980) is applied, which includes the solution of an additional prognostic equation for the subgrid-scale

TKE. Moreover, the discretization for space and time is done by a fifth-order advection scheme after Wicker and Skamarock (2002) and a third-order Runge-Kutta time-step scheme (Williamson, 1980), respectively. The interested reader is referred to Maronga et al. (2015) for a detailed description of the PALM model.

In order to account for radiative effects on fog and the Earth's surface energy balance, the radiation code RRTMG (Clough et al., 2005) has been recently coupled to PALM, running as an independent single column model for each vertical column of the LES domain. RRTMG calculates the radiative fluxes (shortwave and longwave) for each grid volume while considering profiles of pressure, temperature, humidity, liquid water, the droplet number concentration (n_c), and effective droplet radius (r_{eff}). Compared to the precursor study of Maronga and Bosveld (2017), improvements in the microphysics parameterization introduced in the scope of the present study allow a more realistic calculation of the fog's radiation budget as n_c is now represented as a prognostic quantity instead of the previously fixed value specified by the user. This involves an improved calculation of r_{eff}, which is given as

$$r_{eff} = \left(\frac{3\, q_l\, \rho}{4\pi\, n_c \rho_l} \right)^{\frac{1}{3}} \exp(\log(\sigma_g)^2), \tag{1}$$

where q_l is the liquid water mixing ratio, ρ the density of air, ρ_l being density of water and $\sigma_g = 1.3$ being the geometric standard deviation of the droplet distribution. The effective droplet radius is the main interface between the optical properties of the cloud and the radiation model RRTMG. Note, that 3D radiation effects of the cloud are not implemented in this approach, which, however, could affect the fog development at the lateral edges during formation and dissipation phases when no homogeneous fog layer is present. As radiation calculations traditionally require enormous computational time, the radiation code is called at fixed intervals on the order of 1 min.

Moreover, PALM's land surface model (LSM) is used to calculate the surface fluxes of sensible and latent heat. The LSM consists of multi-layer soil model, predicting soil temperature and soil moisture, as well as a solver for the energy balance of the Earth's surface using a resistance parameterization. The implementation is based on the ECMWF-IFS land surface parametrization (H-TESSEL) and its adaptation in the DALES model (Heus et al., 2010). A description of the LSM and a validation of the model system for radiation fog is given in Maronga and Bosveld (2017).

2.2 Bulk microphysics

As a part of this study, the two-moment microphysics scheme of Seifert and Beheng (2001; 2006) implemented in PALM, basically only predicting the rain droplet number concentration (n_r) and cloud water mixing (q_r), was extended by prognostic equations for n_c and cloud water mixing ratio (q_c). The scheme of Seifert and Beheng (2001; 2006) is based on the separation of the cloud and rain droplet scale by using a radius threshold of 40 µm. This separation is mainly used for parameterizing coagulation processes by assuming different distribution functions for cloud and rain droplets. However, as collision and coalescence are weak in fog due to small average droplet radii, the production of rain droplets is negligible. Consequently, only the number concentration and mixing ratio of droplets (containing all liquid water and thus abbreviated with q_l here) are considered in the following. The budgets of the cloud water mixing ratio and number concentration are given

by

$$\frac{\partial q_l}{\partial t} = -\frac{\partial u_i q_l}{\partial x_i} + \left(\frac{\partial q_l}{\partial t}\right)_{\text{activ}} + \left(\frac{\partial q_l}{\partial t}\right)_{\text{cond}} - \left(\frac{\partial q_l}{\partial t}\right)_{\text{auto}} - \left(\frac{\partial q_l}{\partial t}\right)_{\text{accr}} - \left(\frac{\partial q_l}{\partial t}\right)_{\text{sedi}}, \tag{2}$$

$$\frac{\partial n_c}{\partial t} = -\frac{\partial u_i n_c}{\partial x_i} + \left(\frac{\partial n_c}{\partial t}\right)_{\text{activ}} - \left(\frac{\partial n_c}{\partial t}\right)_{\text{evap}} - \left(\frac{\partial n_c}{\partial t}\right)_{\text{auto}} - \left(\frac{\partial n_c}{\partial t}\right)_{\text{accr}} - \left(\frac{\partial n_c}{\partial t}\right)_{\text{sedi}}. \tag{3}$$

The terms on the right-hand side represent the decrease or increase by advection, activation, diffusional growth, autoconversion,
5   accretion, and sedimentation (from left to right). Following Ackerman et al. (2009), cloud water sedimentation is parameterized
assuming that droplets are having a log-normal distribution and are following a Stokes regime. This results in a sedimentation
flux of

$$F_{q_l} = k_F \left(\frac{4}{3}\pi\rho_l n_c\right)^{-2/3} (\rho q_l)^{\frac{5}{3}} \exp(5\ln^2\sigma_g), \tag{4}$$

with the parameter ~~$k = 1.2 \cdot 10^8$~~ $k_F = 1.2 \cdot 10^8$ m^{-1}s^{-1} (Geoffroy et al., 2010). The main focus of this paper is to study the
10   effect of different microphysical parameterizations of activation and condensation processes on microphysical and macroscopic
properties of radiation fog. Those different activation and ~~condensation~~ supersaturation parameterizations will be discussed in
the following.

2.2.1   Activation

It is well known that the aerosol distribution and the activation process are of great importance ~~to~~ for the life cycle of fog
15   (e.g. Gultepe et al., 2007). The amount of activated aerosols determines the number concentration of droplets within the fog,
which~~in turn~~, in turn, has a significant influence on radiation through optical thickness as well as on sedimentation and
consequently ~~influences~~ affects macroscopic properties of the fog, ~~such as its vertical extension~~like for instance its vertical
extent. For these reasons, a sophisticated treatment of the activation process is an essential prerequisite for the simulation of
radiation fog. ~~Several~~ Several activation parameterizations for bulk microphysics models have been ~~developed to provide a~~
20   ~~realistic activation model~~proposed in literature. In this work, three of these activation schemes were compared with each other
in order to quantify their ~~influence~~ effect on the development of a radiation fog event. The schemes considered in this scope are
the ~~simple~~ activation scheme of Twomey (1959) which was used, e.g., by Bott and Trautmann (2002) to simulate radiation fog,
the scheme of Cohard et al. (1998) (used by e.g. Stolaki et al., 2015; Mazoyer et al., 2017) and the one by Khvorostyanov and
Curry (2006). The latter two represent an empirical and analytically extension of Twomeys scheme, respectively. Consequently,
25   these parameterizations are frequently termed Twomey-type parameterizations ~~with the general type of~~that have the following
form:

$$N_{\text{CCN}}(s) = N_0 s^{k}, \tag{5}$$

where N_{CCN} are the number of activated cloud condensation nuclei (CCN), N_0 and ~~k~~ k are parameters depending on the aerosol
distribution, and s is the supersaturation. ~~This equation can be solved using several approaches and mathematical complexity~~
30   ~~levels. In the following, these three schemes and their underlying equations are presented.~~The three parameterizations considered
in the present study are variations of Eq. 5 differing in mathematical complexity:

1. **Twomey (1959):** The ~~simple~~ power law expression (~~see~~ Eq. 5) is well known and has been used for decades to estimate the number of activated aerosol for a given air mass in dependence of the supersaturation. A weakness of this approach is that the parameters N_0 and k are usually assumed to be constant and are not directly linked to the microphysical properties. Furthermore, this relationship creates an unbounded number of CCN at high supersaturations.

2. **Cohard et al. (1998):** extended Twomey's power law expression by using a more realistic four-parameter CCN activation spectrum as shaped by the physiochemical properties of the accumulation mode. Although an extension to the multi-modal representation of an aerosol spectrum would be possible, all relevant aerosols that are activated in typical supersaturations within clouds and especially fog are represented in the accumulation mode (Cohard et al., 1998; Stolaki et al., 2015). Following Cohard et al. (1998) and Cohard and Pinty (2000) the activated CCN number concentration is expressed by

$$N_{\mathrm{CCN}}(s) = Cs^k \cdot F\left(\mu, \frac{k}{2}, \frac{k}{2}+1; \beta s^2\right), \tag{6}$$

~~while~~ where C is proportional to the total number concentration of CCN that is activated when supersaturation s tends to infinity. ~~Parameters~~ Beside k, the parameters μ, and β are adjustable shape parameters associated with the characteristics of the aerosol size spectrum such as geometric mean radius and the geometric standard deviation as well as with chemical composition and solubility of the aerosols. Thus, in contrast to ~~a simple~~ the original Twomey approach, the ~~influence~~ effect of physiochemical properties ~~of~~ on the aerosol spectrum are taken into account.

3. **Khvorostyanov and Curry (2006):** have found an analytical solution to express the activation spectrum using Koehler theory. Therein, it is assumed that the dry aerosol spectrum follows a log-normal size distribution of aerosol f_d:

$$f_d = \frac{dN_a}{dr_\mathrm{d}} = \frac{N_\mathrm{t}}{\sqrt{2\pi}\ln\sigma_\mathrm{d} r_\mathrm{d}} \exp\left[-\frac{\ln^2(r_\mathrm{d}/r_\mathrm{d0})}{2\ln^2\sigma_\mathrm{d}}\right]. \tag{7}$$

Here, r_d is the dry aerosol radius, N_t the total number of aerosols, σ_d is the dispersion of the dry aerosol spectrum, and r_d0 is the mean radius of the dry particles. The number of activated CCN as a function of supersaturation s is then given by

$$N_{\mathrm{CCN}}(s) = \frac{N_\mathrm{t}}{2}[1 - \mathrm{erf}(u)]; \qquad u = \frac{\ln(s_0/s)}{\sqrt{2}\ln\sigma_\mathrm{s}}, \tag{8}$$

where erf is the Gaussian error function, and

$$s_0 = r_\mathrm{d0}^{-(1+\beta)}\left(\frac{4A^3}{27b} \frac{4A_\mathrm{K}^3}{27b}\right)^{1/2}, \qquad \sigma_s = \sigma_\mathrm{d}^{1+\beta}. \tag{9}$$

In this case, ~~A~~ A_K is the Kelvin parameter and b and β depend on the chemical composition and physical properties of the soluble part of the dry aerosol.

Since prognostic equations were neither considered for the aerosols nor their sources and sinks, a fixed aerosol background concentration was prescribed by setting parameters N_0, C and N_t for the three activation schemes. The different nomenclature of the aerosol background concentration is based on the nomenclature used in the original literature.

The activation rate is then calculated as

$$\left(\frac{\partial n_\text{c}}{\partial t}\right)_{activ} = \max\left(\frac{N_\text{CCN} - n_\text{c}}{\Delta t}, 0\right), \tag{10}$$

where n_c is the number of previously activated aerosols that are assumed to be equal to the number of pre-existing droplets and Δt is the length of the model time step. ~~It should be noted~~ Note that this method does not ~~represent the~~ take into account
5 reduction of CCN. However, this error can be neglected since processes as aerosol washout and dry deposition are of minor importance for radiation fog. For all activation schemes it is assumed that every activated CCN becomes a droplet with an initial radius of 1 µm. This results in a change of liquid water, which is considered by the condensation scheme and is described in the next section. Furthermore, we performed a sensitivity study with initial radii of 0.5 µm to 2 µm, which showed that the choice of the initial radius had no impact on the results (not shown). This is consistent with the findings of Khairoutdinov and
10 Kogan (2000) and Morrison and Grabowski (2007).

2.2.2 Condensation and supersaturation calculation

The representation of diffusional growth, evaporation, and calculating the underlying supersaturation (which is the main driver for activation) is one of the fundamental tasks of cloud physics. Three different methods have been evaluated and widely discussed in the scientific community. Namely these are the saturation adjustment scheme, the ~~simple explicit~~ diagnostic scheme,
15 where the supersaturation is ~~derived~~ diagnosed by the prognostic fields of temperature and water vapor, and a prognostic ~~calculation method of~~ method for calculating the supersaturation following ~~(e.g. Clark, 1973; Morrison and Grabowski, 2007; Lebo et al., 2~~ e.g. Clark (1973); Morrison and Grabowski (2007); Lebo et al. (2012). Basically, the supersaturation is given by $s = q_\text{v}/q_\text{s} - 1$, while the absolute supersaturation (or water vapor surplus) is defined as $\delta = q_\text{v} - q_\text{s}$, where q_v is the water vapor mixing ratio and q_s is the saturation mixing ratio. In the following, these three methods are ~~reviewed briefly~~ briefly reviewed.

20 1. **Saturation adjustment:** In many microphysical models, a saturation adjustment scheme is applied. The basic idea of this scheme is that all supersaturation is removed within one model time step and supersaturations are thus neglected~~; and~~. Saturation adjustment thus potentially leads to excessive condensation. Despite the many years of application of this scheme, its ~~influence~~ impact on microphysical processes is discussed controversially ~~in the community~~ (e.g. Morrison and Grabowski, 2008; Thouron et al., 2012; Lebo et al., 2012). Saturation adjustment might hence especially be a source
25 of error in fog simulations where very small time steps are used due to small grid spacings as ~~outlined earlier~~ already discussed. Using the saturation adjustment scheme, q_l represents a diagnostic value calculated by means of

$$q_\text{l} = \max(0, q - q_\text{r} - q_\text{s}), \tag{11}$$

where q is the total water mixing ratio. The saturation mixing ratio, which is a function of temperature, is approximated in a first step by

30 $$q_\text{s}(T_\text{l}) = \frac{R_\text{d}}{R_\text{v}} \frac{e_\text{s}(T_\text{l})}{p - e_\text{s}(T_\text{l})}, \tag{12}$$

where T_l is the liquid water temperature and p is pressure. ~~The individual~~ R_d and R_v are the specific gas constants for dry air and water vapor ~~are denoted R_d and R_v~~, respectively. For the saturation vapor pressure (e_s) an empirical relationship of Bougeault (1981) is used. In a second step, q_s is corrected using a first-order Taylor series expansion of q_s:

$$q_s(T) = q_s(T_l) \frac{1 + \beta q}{1 + \beta q_s(T_l)} \frac{1 + \gamma q}{1 + \gamma q_s(T_l)}, \tag{13}$$

with

$$\beta\gamma = \frac{L_v}{R_v c_p T_l^2}, \tag{14}$$

where c_p is the specific heat of dry air at constant pressure and L_v is the latent heat of vaporization. As aforementioned, in each model time step, all supersaturation is converted into liquid water or, in subsaturated regions, the liquid water is reduced until saturation. ~~Therefore, for using the saturation adjustment scheme and a calculation of aerosol activation , the supersaturation must be estimated. For that, using~~ In order to use this scheme with aerosol activation parameterizations, it is necessary to estimate the supersaturation (see Eq. 5). This can be achieved for the activation scheme of Cohard et al. (1998) ~~the supersaturation is estimated following Thouron et al. (e.g. 2012); Mazoyer et al. (e.g. 2017); Zhang et al. (e.g. 2014) and directly translated~~ following e.g. Thouron et al. (2012); Mazoyer et al. (2017); Zhang et al. (2014) and directly translating into a droplet number concentration by

$$s^{k+2} \cdot F\left(\mu, k/2, k/2+1, -\beta s\right) = \frac{\left(\phi_1 w + \phi_3 \frac{dT}{dt}|_{\mathrm{rad}}\right)^{3/2}}{2kC\pi\rho_l\phi_2 B(k/2, 3/2)} \frac{\left(\phi_1 w + \phi_3 \frac{dT}{dt}|_{\mathrm{rad}}\right)^{\frac{3}{2}}}{2kC\pi\rho_l\phi_2 B\left(\frac{k}{2}, \frac{3}{2}\right)}, \tag{15}$$

where ϕ_1, ϕ_2 and ϕ_3 are functions of temperature and pressure and given in Cohard et al. (1998) and Zhang et al. (2014). w is the vertical velocity and B the beta function.

2. ~~**Explicit**~~ **Diagnostic supersaturation calculation:** Supersaturation is calculated ~~explicitly~~ diagnostically from q_v and temperature T (from which q_s can be derived). However, since it is assumed that the supersaturation is kept constant during one model time step, the ~~explicit~~ diagnostic approach requires a very small model time step of

$$\Delta t \leq 2\tau, \tag{16}$$

due to stability reasons (Árnason and Brown Jr, 1971). Here, τ is the supersaturation relaxation time which is approximated by

$$\tau \approx (4\pi D n_c \underline{r}\bar{r})^{-1}, \tag{17}$$

where ~~$\langle r \rangle$~~ $\bar{r}$ is the average droplet radius, and D the diffusivity of water vapor in air. Due to the low dynamic time step in the present study imposed by the Courant-Friedrichs-Lewy criterion (on the order of 0.1 s), however, the condensation time criterion is fulfilled, and no additional ~~reduction of the time step~~ time step decrease is needed. The rate of cloud

water change due to condensation or evaporation is given by

$$\left(\frac{\partial q_{\mathrm{l}}}{\partial t}\right)_{\mathrm{cond}} = \frac{4\pi G(T,p)\rho_{\mathrm{w}}}{\rho_{\mathrm{a}}}s\int_{0}^{\infty}rf(r)dr \tag{18}$$

$$= \frac{4\pi G(T,p)\rho_{\mathrm{w}}}{\rho_{\mathrm{a}}}sr_{\mathrm{c}} \tag{19}$$

where r_{c} is the integral radius and $G = \frac{1}{F_{\mathrm{K}}+F_{\mathrm{D}}}$ included the thermal conduction and the diffusion of water vapor (Khairoutdinov and Kogan, 2000). The density ratio of liquid water and the solute is given by $\rho_{\mathrm{w}}/\rho_{\mathrm{a}}$. ~~Using such a small time step allows the use of a diagnostic approach for the supersaturation calculation.~~

3. **Prognostic supersaturation:** The prognostic ~~/ semi-analytic~~ approach, which was first introduced by Clark (1973), includes an additional prognostic equation for the absolute supersaturation. Even though this requires ~~further computational costs for~~ solving one more prognostic equation, it mitigates the problem of spurious cloud-edge supersaturations and prevent inaccurate supersaturation caused by small errors in the advection of heat and moisture ~~(Morrison and Grabowski, 2007; Thouron~~ (Morrison and Grabowski, 2007; Grabowski and Morrison, 2008; Thouron et al., 2012).

The temporal change of ~~the absolute supersaturation~~ δ is given by

$$\frac{\partial \delta}{\partial t} - \frac{1}{\rho}\nabla \cdot (u\,\rho\delta) = A - \frac{\delta}{\tau}, \tag{20}$$

with ~~A~~ A described by

$$A = -q_{\mathrm{s}}\frac{\rho g w}{p - e_{\mathrm{s}}} - \frac{dq_{\mathrm{s}}}{dT}\cdot\left[\frac{gw}{c_{\mathrm{p}}} + \left(\frac{dT}{dt}\right)_{\mathrm{rad}}\right], \tag{21}$$

with g being gravitational acceleration. The supersaturation relaxation time is given in Eq. 17. The second term on the left hand side of Eq. 20 describes the change of the absolute supersaturation due to advection, while the right hand side considers ~~effects for~~ changes of δ ~~due to~~ to changes in pressure, adiabatic compression/expansion, and radiative effects (from left to right). By doing so, the predicted supersaturation is used for determining the number of activated droplets as well as the condensation and evaporation processes. Note that here the absolute supersaturation is taken, as using s would involve more terms and is more complex to solve (Morrison and Grabowski, 2007).

3 Case description and model setup

The simulations performed in the present study are based on an observed deep fog event during the night from 22 to 23 March 2011 at the Cabauw Experimental Site for Atmospheric Research (CESAR). The fog case is described in detail in Boers et al. (2013) and was used as validation case for PALM ~~in~~ byMaronga and Bosveld (2017). The CESAR site is dominated by rural grassland landscape and, although it is relatively close to the sea, ~~there are typically~~ continental aerosol conditions are commonly observed and are characterized by agricultural processes (Mensah et al., 2012).
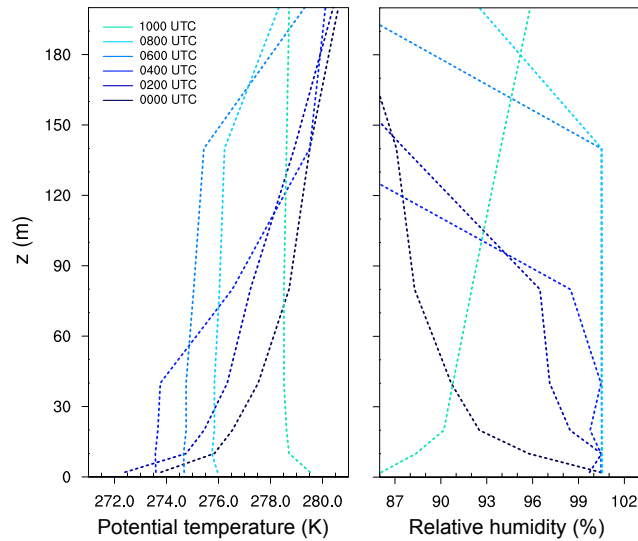
Figure 1. Profiles of potential temperature and relative humidity at different times as observed at Cabauw.

The fog initially formed at midnight (as a thin near-surface layer), induced by radiative cooling, which also produced a strong inversion with a temperature gradient of 6 K between the surface and the 200 m tower-level. In the following, the fog layer began to develop: ~~At~~ at 0300 UTC the fog had a vertical extension of less than 20 m, then deepened rapidly to 80 m, and reaching 140 m depth at 0600 UTC. At 0300 UTC, also the visibility had reduced to less than 100 m. After sunset (around 0545 UTC) a further invigoration close to the ground was suppressed and after 0800 UTC the fog starts quickly evaporate due to direct solar heating of the surface. For details, see Boers et al. (2013).

The model was initialized as described in the precursor study of Maronga and Bosveld (2017). Profiles of temperature and humidity (see Fig. 1) were derived from the CESAR 200 m-tower and used as initial profiles in PALM. A geostrophic wind of $5.5 \, \mathrm{m \, s^{-1}}$ was prescribed based on the observed value at Cabauw at 0000 UTC.

The land surface model was initialized with short grassland as surface type and four soil model layers at the depths of 0.07 m, 0.28 m, 1.0 m and 2.89 m. The measured surface layer temperatures were interpolated to the respective levels, resulting in temperatures of 279.54, 279.60, 279.16, and 279.16 K for soil layers one to four, respectively. Furthermore, the initial soil moisture was set to the value at field capacity ($0.491 \, \mathrm{m^3 m^{-3}}$), which reflects the very wet soil and low water table in the Cabauw area. ~~The heat conductivity was set to $\Lambda = 4$, based on the radiation and energy balance observed at 0000 UTC at Cabauw.~~ Moreover, the roughness length for momentum was prescribed to 0.15 m. Note that Maronga and Bosveld (2017) discussed that this value appears to be a little high given the season and wind direction. This does not play an important role for the present study, however, as we will not focus on direct comparison against observational data from Cabauw.

All simulations start at 0000 UTC, before fog formation, and end at 1015 UTC on the next morning after the fog layer has fully dissipated. Precursor runs are conducted for additional 25 min using the initial state at 0000 UTC, but without radiation
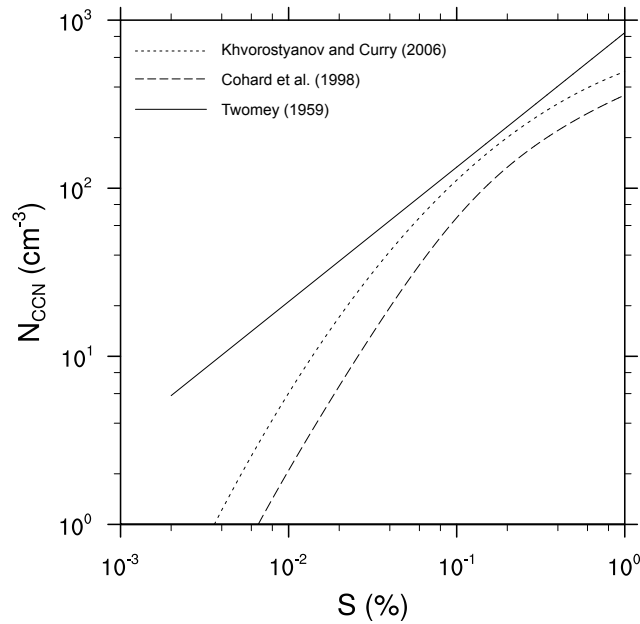
10

Figure 2. Activation spectrum for three different activation schemes of Twomey (1959), Cohard et al. (1998) and Khvorostyanov and Curry (2006) for a typical continental aerosol environment.

scheme and LSM in order to allow the development of turbulence in model without introducing feedback during that time (see Maronga and Bosveld, 2017).

Based on sensitivity studies of Maronga and Bosveld (2017), a grid spacing of $\Delta = 1\,\mathrm{m}$ was adopted for all simulations, with a model domain size of 768 x 768 x 384 grid points in x-, y-, and z-direction, respectively. Cyclic conditions were used

5   at the lateral boundaries. A sponge layer was used starting at a height of 344 m in order to prevent gravity waves from being reflected at the top boundary of the model.

~~Tab.1 gives on overview over~~ Table 1 gives an overview of the simulation cases. All cases were initialized with (identical) continental aerosol conditions. Case SAT represents a reference run with no activation scheme and thus a prescribed constant value of $n_{\mathrm{c}} = 150\,\mathrm{cm}^{-3}$ (estimated from simulations of ~~Boers et al. (2013)~~Boers et al., 2013). This case represents ~~a similar~~ the

10 same setup to the one described in Maronga and Bosveld (2017) except of modifications concerning the aerosol environment as outlined below. Condensation processes were here treated with the saturation adjustment scheme (Seifert et al., 2006). In order to evaluate the influence of saturation adjustment in a one-moment microphyiscs scheme on the development of radiation fog, identical assumptions were made in case ~~EXP~~ DIA and PRG, except that ~~diffusion~~ diffusional growth was calculated with the ~~explicit~~ diagnostic and prognostic method, respectively (see section 2.2.2).

15 Moreover, as small differences in supersaturation can effect the number of activated droplets significantly the impact of different methods for calculating supersaturation on CCN activation is investigated in a two-moment microphysics approach

(see section 4.2.2). Therefore, the simulation N2SAT, ~~respectively. Cases N1EXP-N3EXP~~ N2DIA and N2PRG were compared to each other. In all three cases the activation scheme of Cohard et al. (1998) is used and initialized as described below.

Furthermore, cases N1DIA-N3DIA used the activation schemes described in chapter 2.2.1. To ensure comparability between the different schemes, all of them were initialized with a continental aerosol background described in Cohard et al. (1998), which is characterized by an aerosol with the chemical composition of ammonium sulfate [$(NH_4)_2SO_4$], a background aerosol concentration of $842\,cm^{-3}$, a mean dry aerosol radius of $r_{d0} = 0.0218\,\mu m$, and a dispersion parameter of the dry aerosol spectrum of $\sigma_d = 3.19$. For the Twomey activation scheme this results in $N_0 = 842\,cm^{-3}$ and $k = 0.8$ which is a typical value for the exponent for continental air masses (e.g. Pruppacher and Klett, 1997, pages 289 et seq.). The Twomey activation scheme does not allow for taking aerosol properties into account. In contrast, the activation scheme of Cohard et al. (1998) requires the parameters C, k, β and μ to be derived from the aerosol properties. Here, values of $C = 2.1986 \cdot 10^6\,cm^{-3}$, $k = 3.251$, $\beta = 621.689$ and $\mu = 2.589$ were used as described in Cohard and Pinty (2000). Finally, the activation scheme of Khvorostyanov and Curry (2006) can directly consider the aerosol properties, which are prescribed as aforementioned. Using those different parameterizations resulting in different activation spectra, which are shown in Fig. 2. One can see, that especially the CCN concentration is changed by using these different methods, such that this part of the study is equivalent to sensitivity study of different CCN concentration but realized by using different coexisting parameterizations. ~~Since changing other microphysical properties (such as mean geometric radius, chemical composition, or dispersion of dry aerosol spectrum) will have a similar effect to the physical outcomes as the variation of the aerosol concentration (because only cloud number concentration is affected), further simulation cases were omitted. Moreover, for investigating the impact of the supersaturation calculation on CCN activation (see section 4.2.2) the simulation N2SAT, N2EXP and N2PRG were compared to each other. In all three cases the activation scheme of Cohard et al. (1998) is used.~~

4 Results

4.1 General fog life cycle and macrostructure

The reference case SAT is conducted with a constant droplet number concentration of $n_c = 150\,cm^{-3}$. The deepening of the fog layer can be seen in Fig. 3, which shows the profiles of the potential temperature, relative humidity and liquid water mixing ratio at different times.

The fog onset is at 0055 UTC, defined by a visibility below 1000 m and a relative humidity of 100%. In the following the fog layer deepens and extends to a top of approximately 20 m at 0200 UTC. However, at this point the stratification of the layer is still stable with a temperature gradient of 6 K between the surface and the fog top. The persistent radiative cooling of the surface and the fog layer leads to a further vertical development of the fog, which is accompanied with a regime transition from stable to convective conditions within the fog layer (see Fig. 3a). This starts as soon as the fog layer begins to become optically thick (at 0330 UTC), and when radiative cooling at the fog top becomes the dominant process, creating a top-down convective boundary layer. The highest liquid water mixing ratio of $q_l = 0.41\,g\,kg^{-1}$ is achieved at 0600 UTC at a height of 60 m (see Fig. 3c), while the ~~the~~ fog layer in total reaches the maximum one hour later at 0700 UTC. The lifting of the fog,

Table 1. Overview of conducted simulations. The droplet number concentration n_c is only prescribed for simulations without activation scheme. In the simulations ~~N1EXP-N3EXP~~ N1DIA-N3DIA n_c is a prognostic quantity and thus variable in time and space. The aerosol background concentration is abbreviated with $N_{a,tot}$, and used to initialize the activation schemes. Note for the scheme ~~of (Cohard et al., 1998)~~ after Cohard et al. (1998) a conversion to the parameter C must be applied, while for both other activation schemes this value is directly used to prescribe N_0 and N_t, respectively.

#	Simulation	Activation scheme	n_c [cm^{-3}]	$N_{a,tot}$ [cm^{-3}]	Condensation scheme
1	SAT	none	150	none	saturation adjustment
2	~~EXP~~ DIA	none	150	none	~~explicit~~ diagnostic
3	PRG	none	150	none	prognostic
4	~~N1EXP~~ N2SAT	~~Twomey (1959)~~ Cohard et al. (1998)	not fixed	842	~~explicit~~ saturation adjustment
5	~~N2EXP~~ N2DIA	Cohard et al. (1998)	not fixed	842	~~explicit~~ diagnostic
6	~~N3EXP~~ N2PRG	~~Khvorostyanov and Curry (2006)~~ Cohard et al. (1998)	not fixed	842	~~explicit~~ prognostic
7	~~N2SAT~~ N1DIA	~~Cohard et al. (1998)~~ Twomey (1959)	not fixed	842	~~saturation adjustment~~ diagnostic
8	~~N2PRG~~ N3DIA	~~Cohard et al. (1998)~~ Khvorostyanov and Curry (2006)	not fixed	842	~~prognostic~~ diagnostic

Figure 3. Profiles of potential temperature (a), relative humidity (b) and liquid water mixing ratio (c) at different times for the reference case REF.

which is defined by a non-cloudy near-surface layer ($q_l \leq 0.01\,\mathrm{g\,kg^{-1}}$), occurs at 0845 UTC. At 1130 UTC the fog is completely dissipated.
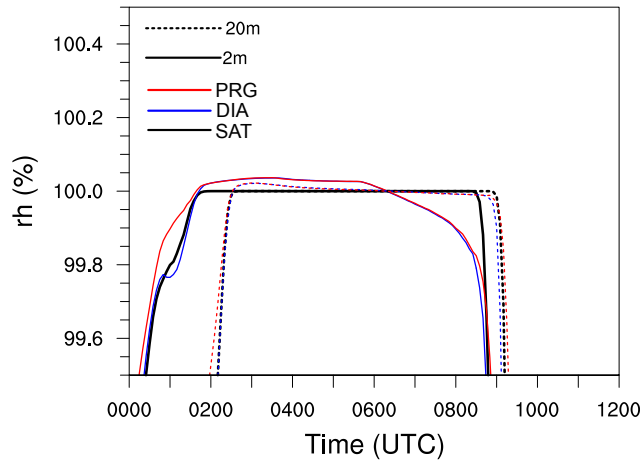
Figure 4. Time series of horizontal-averaged relative humidity/supersaturation at height levels of 2 m (~~dotted~~solid) and 20 m (~~dashed~~dotted) for different methods in treating the supersaturation calculation.

4.2 Influence of different supersaturation ~~parameterizations on diffusional growth~~calculation

In this section we discuss the influence of three different method considering supersaturation. Namely these are (as aforementioned) saturation adjustment, a diagnostic supersaturation calculation and a prognostic method. In the first subsection a one-moment microphysic scheme is used and the impact of the different supersaturation methods is limited to the effect of diffusional
5   growth. In the second part of this study those methods are applied in a two-moment microphysics scheme and considering the effect of such different approaches of supersaturation calculations for activation.

4.2.1 One-moment microphysics scheme: impact of supersaturation calculation on diffusional growth

In this section we discuss the error introduced by using saturation adjustment for simulating radiation fog with a one-moment scheme in a LES. For this, we compare three simulations with identical setup (cases SAT, ~~EXP~~DIA, and PRG), which differs
10   only in the way how supersaturation is calculated and consequently the amount of condensed or evaporated liquid water. To isolate this effect, activation is neglected in all cases and n_c is set to a constant value of $150\,\mathrm{cm}^{-3}$ (a typical value in fog layers). The effect on different supersaturations driving the diabatic process of activation is discussed in section 4.2.2. ~~Due to the small grid spacing of 1 m used in our simulations,~~ As mentioned before the time step is ~~in the order of 10^{-1}~~roughly 0.1 s, which is more than one order of magnitude smaller than the allowed values of ~~2-5~~2 - 5 s for assuming saturation adjustment (Thouron
15   et al., 2012). The present case hence is an ideal environment evaluating the error introduced by using saturation adjustment and by keeping all other parameters fixed.

    Figure 4 shows time series of the horizontally-averaged saturation (supersaturation) for ~~SAT, EXP and PRG case~~cases SAT, DIA and PRG at selected heights close to the surface. In all cases saturation occurs simultaneously around 0120 UTC. In case SAT, relative humidity does not exceed 100% due to its limitation by saturation adjustment, while in case ~~EXP~~DIA and
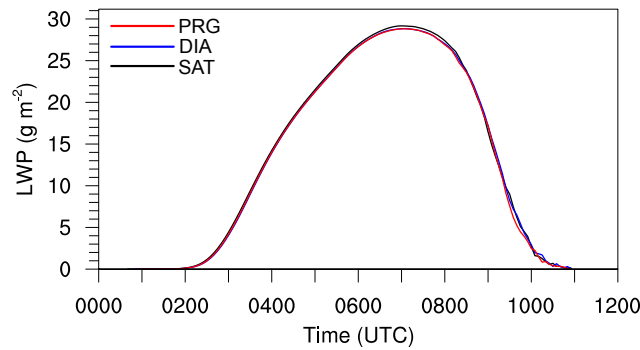
14

Figure 5. Time series of liquid water path (LWP) for cases using saturation adjustment, the ~~explicit~~ diagnostic approach and a prognostic method for the diffusional growth.

PRG average supersaturations of 0.05% ~~in~~ are reached at a height of 2 m~~occur~~, which corresponds to typical values within fog ~~(Hammer et al., 2014; Mazoyer et al., 2017; Boutle et al., 2018)~~(Hammer et al., 2014; Mazoyer et al., 2019; Boutle et al., 2018).

For ~~case EXP~~ cases DIA and PRG starting from 0615 UTC (in 2 m height) and 0715 UTC (in 20 m height), supersaturations are removed and the air becomes subsaturated (on average). This is in contrast with case SAT, where the saturation adjustment approach keeps the relative humidity at 100% as long as liquid water is present (i.e. until the fog has dissipated). Around 0600 UTC, which is shortly after sunrise, relative humidity drops rapidly in PRG and DIA as a direct consequence of direct solar heating of the surface and the near-surface air, preventing further supersaturation at these heights. While we cannot clearly identify the lifting of the fog in case ~~EXP~~ DIA and PRG (due to the limited humidity range displayed), we note that for case SAT we can identify lifting times as a decrease of relative humidity around 0845 UTC at 2 m height and around 0910 UTC at 20 m height.

Beside this inherent difference in relative humidity, the general time marks ~~(formation, lifting, dissipation, defined as in Maronga and Bosveld (2017))~~ (formation, lifting, dissipation, defined by Maronga and Bosveld, 2017) of the fog layer are identical for cases SAT, ~~EXP~~ DIA and PRG.

~~Instantaneous horizontally averaged profiles for the liquid water mixing ratio (left) for 0400 UTC, 0600 UTC and 0800 UTC and budgets for q_l tendencies (right, upper row: condensation and evaporation, middle row: sedimentation and advection and lower row: total tendency) for 0400 UTC, 0600 UTC and 0800 UTC for the simulations SAT, EXP and PRG.~~

Figure 5 shows the liquid water path (LWP) for all cases. Differences in the LWP appear between 0400 UTC and 1100 UTC and do not exceed 1% (lower values for cases ~~EXP~~ DIA and PRG), indicating that the choice of the condensation scheme does not affect the total water content of the simulated fog layer.

4.2.2 ~~Budget of liquid water~~

~~Fig. ?? shows profiles for~~

15

It can be summarized that, although the assumptions of saturation adjustment are not valid for the simulation of fog when using a very small time step, the mean liquid water content is not changed by more than 1% and the general fog structure is not altered when using a one-moment microphysics and neglecting supersaturation. This is probably due to the very small supersaturation that is not strong enough to generate a significant change in the effective droplet radius, and which could possibly lead to stronger sedimentation or higher radiative cooling rates.

4.2.2 Two-moment microphysics scheme: impact of supersaturation calculation on CCN activation

Even though different methods for calculating supersaturation which interacts with the diffusional growth are not strong enough to generate any noteworthy differences by using a one-moment microphysics (considering a constant value for n_c) the impact of different methods modelling supersaturation on CCN activation by using a two-moment microphysics might be significant.

Figure 6 shows the LWP for simulations applying the activation scheme of Cohard et al. (1998) in conjunction with the usage of saturation adjustment (N2SAT), the diagnostic scheme (N2DIA), and the prognostic scheme (N2PRG) for calculating supersaturations. It can be seen that the prognostic and diagnostic methods produce similar LWP values. However, for case N2SAT the LWP is nearly 70% higher than for the other two cases. In Fig. 7 profiles of the liquid water mixing ratio (left) and droplet number concentration (right) are shown. From that figure it can be seen that in case of N2SAT both the fog height as well as the liquid water ~~budgets at 0400~~ mixing ratios within the layer are higher than in N2DIA and N2PRG, respectively. However, small differences in q_l can also be found between N2DIA and N2PRG (e.g. at 0600 UTC ~~,~~ in the second third of the fog layer). This is explained by slightly higher values for the number concentration in case of N2DIA than in N2PRG. However, both are at approximately $75\,\text{cm}^{-3}$ at 0600 UTC ~~and 0800~~. In contrast, in simulation N2SAT a number concentration of 120 ~~UTC for cases SAT, EXP and PRG. These times represent different stages of the fog development: deepening, mature phase,~~ cm^{-3} to $150\,\text{cm}^{-3}$ (at the top) is observed, which is about 60%-100% higher in comparison to N2DIA and N2PRG. These differences can be explained by the different methods for calculating the supersaturation, since activation is the main process altering the droplet number concentration. Therefore, we can implicitly derive from the droplet number concentration that the predicted and diagnosed supersaturations using the prognostic and diagnostic method are similar. These differences between N2SAT and ~~mature phase development after sunrise, respectively. Figure ??a confirms that especially at the top of the fog, when it becomes radiative active, the liquid water is slightly higher in the case of saturation adjustment , but in general the differences between the runs are negligible. Figures ?? (right) show a clear trend: On the one hand the sedimentation and advection rates are almost identical for all cases at all times . On the other hand, clear differences can be observed in the production rate for condensation and the dissipation rate due to evaporation. In the case of saturation adjustment, these rates are almost twice as high (in absolute sense) as for the cases EXP and PRG over the entire height of the fog layer. This finding can be attributed to~~ N2DIA/N2PRG are, however, in good agreement with values reported for a stratocumulus case by Thouron et al. (2012). Their Fig. 2 shows that the ~~fact that saturation adjustment is assuming the highest possible values for condensation. This in turn also affects the evaporation rates, which are counteracting the production by excessive condensation. The net effect, however, is small (c.f. Fig. 5).~~ number concentration of the diagnostic and prognostic method were also similar and the case with saturation adjustment overestimated the supersaturation and therefore the droplet number concentration. As
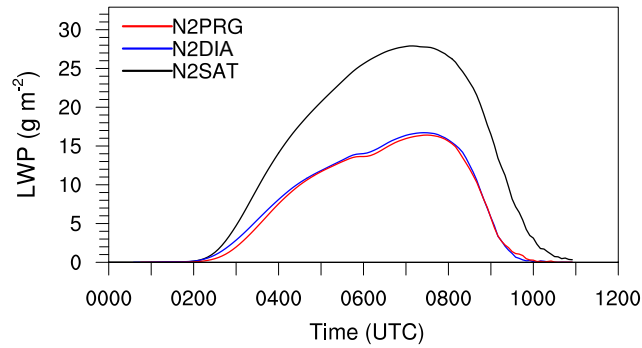
16

Figure 6. Time series of LWP for simulations using saturation adjustment (N2SAT, black), the diagnostic scheme (N2DIA, blue) and the prognostic method (N2PRG, red). All cases uses the activation scheme of Cohard et al. (1998).
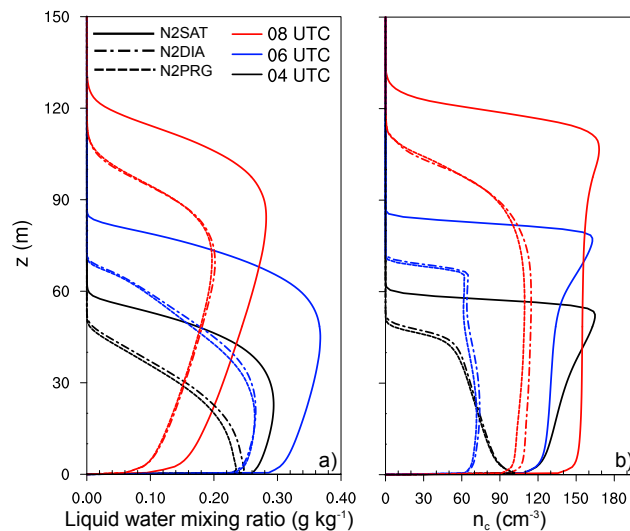

Figure 7. Profiles for liquid water mixing ratio (a) and droplet number concentration (b) at 0400 UTC, 0600 UTC and 0800 UTC.

the fog droplet number concentration has a crucial feedback on the overall LWP of the fog layer, the times of lifting, and the time of its dissipation, the reported differences in n_c are significant regarding the accurate modelling and prediction of fog. The reason why the number concentration is such a critically parameter can be ascribed to their impact on sedimentation and radiative cooling, which is explained in more detail in section 4.4.3.

5   ~~It can be summarized that , although the assumptions of saturation adjustment arenot valid for the simulation of fog when using a very small time step, the mean liquid water content is not changed by more than~~

In order to evaluate the possible effect of the grid spacing, in conjunction with different methods for calculating the supersaturation, on CCN activation, we repeated each of the cases N2SAT, N2DIA, and N2PRG with two coarser grid spacings of 2 m and 4 m. The general effect of the grid spacing on the temporal development and structure of radiation fog is discussed
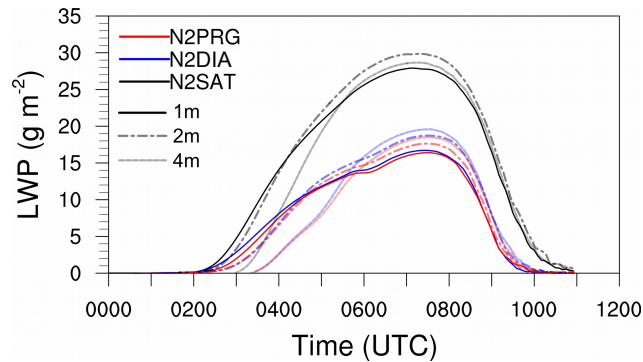
17

Figure 8. As Fig. 6 but also 2 m (dot-dashed) and 4 m (dashed).

in detail in Maronga and Bosveld (2017). In this section, we will focus only on changes in LWP due to different supersaturation calculations at different spatial model resolutions. For isolating the effect of the grid spacing, all simulations with a coarser grid spacing were carried out with the same time step of 0.125 s, which corresponds to the average time step of the simulations at highest grid spacing of 1 ~~%~~ m. In this way, effects of different time steps induced by different grid spacings, could be eliminated.

Fig. 8 shows the LWP for all grid sensitivity runs. First of all, note that for 1 m grid spacing, the results reflect the results shown in Fig. 6 and discussed above (i.e. significantly higher LWP for case N2SAT than for cases N2DIA and ~~the general fog structure is not altered. This is probably due to the very small supersaturation that is not strong enough to generate a significant change in the effective droplet radius, and which could lead to stronger sedimentation or higher radiative cooling rates. But as the different methods calculating supersaturation are not strong enough to create any noteworthy differences in condensational growth by using 1-moment microphysics (keeping the droplet number concentration constant) , the impact of these differences for activation might be crucial and is discussed in section 4.2.2~~N2PRG. Moreover, Fig. 8 reveals that these results are somewhat sensitive to changes in the grid spacing. For all cases we observe a tendency towards higher LWP values with increasing grid spacing, at least for cases N2DIA and N2PRG. These difference are, however, not larger than 4 g m^{-2} and thus significantly smaller than the observed differences found between the different methods to calculate supersaturation. Note, however, that the relative change in LWP with grid spacing is higher for case N2DIA than for case N2PRG. Quantitatively speaking, in case of 1 m grid spacing the relative difference of the LWP is 2.1% between N2DIA and N2PRG during the mature phase while for the case with a grid spacing of 4 m it reaches 8.1%. This might be explained by the fact that the diagnostic scheme is very sensitive to small errors (e.g. induced by the numerical advection) in the temperature and humidity fields (e.g. Morrison and Grabowski, 2008; Thouron et al., 2012). A coarser spatial resolution here can lead to larger error introduced by spurious supersaturation. We thus suppose that the increased differences (see Fig. 8) by larger grid spacings are induced by spurious supersaturation, which affect the CCN activation and hence influence the LWP of the fog layer.
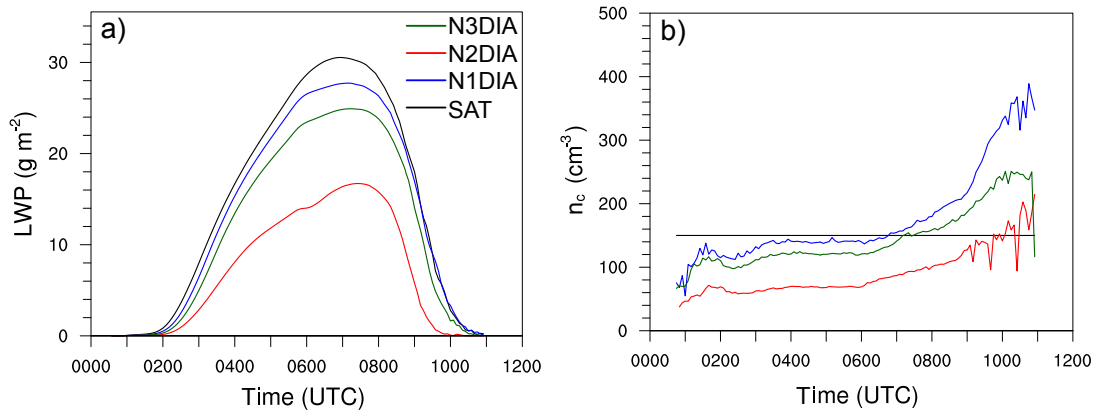
18

Figure 9. Time series of LWP and n_c (as a horizontal and vertical average of the fog layer) for the reference and ~~N1EXP-N3EXP~~ N1DIA-N3DIA case.

Furthermore, we note that coarser grid spacings lead to later fog formation time, which is in agreement with Maronga and Bosveld (2017) and which can be ascribed to under-resolved turbulence near the surface at coarse grids.

In summary, we can thus conclude that the sensitivity to changes in the grid spacing is rather small, but it might imply differences in the LWP of the simulated fog layer of up to $4\,\mathrm{g\,m^{-2}}$.

4.3 ~~Comparison~~ Two-moment microphysics scheme: comparison of different activation parameterizations

In numerous previous studies, the influence of aerosols and the activation process on the life cycle of fog was investigated (e.g. Bott, 1991; Stolaki et al., 2015; Maalick et al., 2016; Zhang et al., 2014; Boutle et al., 2018). Although all three activation schemes outlined in section 2.2.1 are comparable power law parameterizations that are initialized with identical aerosol spectra, the ~~influence on~~ effect on simulations of radiation fog is still unknown~~, since~~. Because changes in n_c due to different activation schemes have ~~considerable effects~~ a considerable effect on the life cycle of fog~~and thus also~~, we might consider that even small differences in n_c might ~~have a significant feedback.~~alter simulated fog layers significantly. This part of the study can be regarded as a sensitivity study of different CCN concentrations realized by applying different activation schemes, which is illustrated also in Fig. 2. However, from a model user's perspective, such a sensitivity is of great importance as CCN concentrations are usually difficult (case studies) or even impossible (forecasting) to obtain and model results thus might highly depend on the chosen activation parameterization.

4.4 LWP and n_c

~~Furthermore, n_c, as a function of time and averaged over the fog volume, is~~ Time series of the LWP for the reference run (case SAT) and the three different cases (N1DIA - N3DIA) are shown in Fig. 9~~b for the reference case and cases N1EXP-N3EXP,~~a. The highest LWP occurs for case SAT which also shows the highest n_c during the formation and mature phase in comparison with the other simulations (see 9b). The time series of n_c shown in 9b (representing runs with the three different aerosol
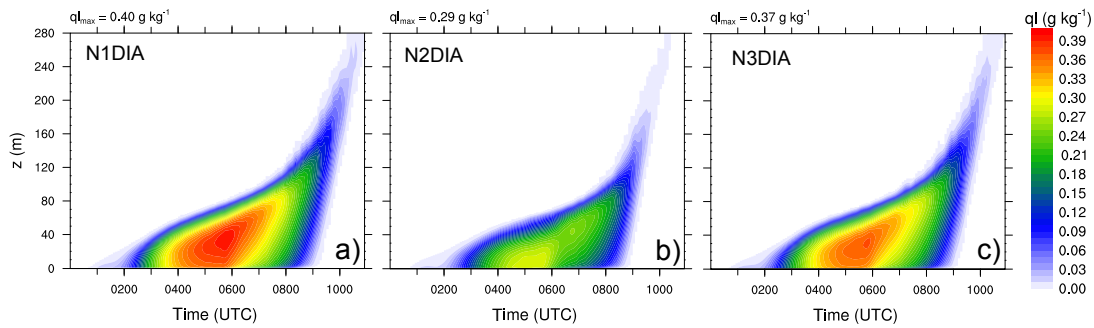
19

Figure 10. Height-time cross sections for the liquid water mixing ratio for ~~N1EXP-N3EXP~~N1DIA-N3DIA.

activation parameterization schemes~~(,~~ see Tab.1) reveal that, depending on the parameterization used, the a shift in n_c towards smaller or larger values is found. The quantitative differences in the number of activated aerosol by using the different activation schemes is ~~explained by~~ due to a slightly different activation spectrum (see ~~Appendix,~~ Fig. 2). A linear relationship between LWP and n_c can be found: a higher n_c leads to higher LWP, which is in agreement to other studies as Boutle et al. (e.g 2018)

5 . In principle, a similar qualitative development of n_c can be observed. While n_c increases during fog formation (with a local maximum with values between 70 and 140 cm^{-3}), it remains nearly constant during the mature phase of the fog ~~. This can be explained by a constant longwave cooling at the fog top , producing similar supersaturations~~(values between 65 and 145 cm^{-3}). We will ~~see later~~ see that activation here happens mostly at the top of the fog, but due to vertical mixing in the convective fog layer, cloud droplets are evenly distributed over a large vertical domain. Furthermore, the mixing layer is increasing in time

10 so that there is no net change of the (averaged) n_c in the fog layer. As soon as the sun rises and the fog layers start to lift and turns into a stratocumulus cloud, all cases show a strong increase in n_c. This increase can be explained by stronger supersaturations induced by thermal updrafts in the developing surface-driven convective boundary layer due to surface heating by solar radiation. Moreover, we note that while the qualitative course of n_c is similar for all cases, the choice of the activation algorithm has an impact on the number of activated aerosols and thus on the strength of the fog-layer~~(see Fig.10),~~ e.g. illustrated

15 in Fig. 10 via q_l. This is due to the radiation effect of the droplets. The number of droplets to which a certain amount of liquid water is distributed plays an important role: the larger the number of droplets, the larger is the radiation-effective surface and the higher also the optical thickness. As a result ~~, on the one hand,~~ the cooling rate ~~from~~ in a fog with many small droplets is increased, allowing more water vapor to condense and the fog to grow stronger. ~~On the other hand, however~~By the same token, sedimentation also depends on the droplet radius and plays a major role ~~that will be discussed later. Time series of the~~

20 ~~LWP for the reference run and the three different cases are shown in Fig. 9a. The highest LWP occurs for the reference run which also shows the highest n_c during the formation and mature phase in comparison with the other simulations. Also for the cases N1EXP-N3EXP a linear relationship between LWP and n_c can be found: A higher n_c leads to higher LWP.~~ for fog development. This will be further discussed below.
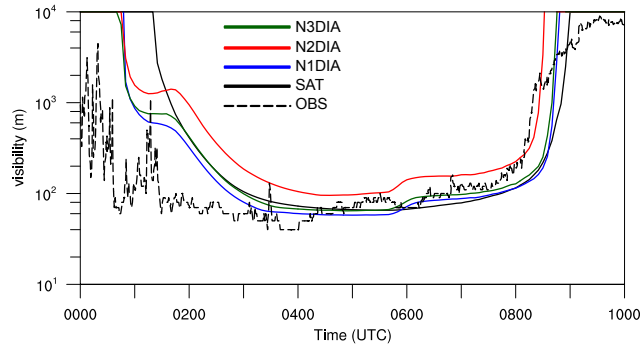
Figure 11. Time series of simulated visibility in 2 m height. Observations from Cabauw (dashed lines) were added for illustration only.

4.4.1 Visibility

In Fig. 11 the simulated visibility for the cases ~~N1EXP-N3EXP~~ N1DIA-N3DIA in 2 m height ~~as well as the observed value is shown~~ together with the observed values at Cabauw (for illustration only). Visibility is calculated from the LES data following ~~following~~ Gultepe et al. (2006) as

$$vis = \frac{1002}{(n_c \, \rho \, q_l)^{0.6473}}, \tag{22}$$

~~(with n_c and q_l~~ with n_c and q_l given in units of cm^{-3} and gm^{-3}, respectively~~). Hence, the visibility is significantly affected by~~. This visibility estimation thus significantly depends on the droplet number concentration and the liquid water content. ~~In contrast to the former part of the study, where the droplet number concentration is a constant value, the analysis of the visibility is interesting here as the activation schemes significantly alter n_c and q_l for the different cases within the fog layer.~~

~~We note~~ Unlike in the first part of this paper, analyzing visibility estimations from the simulations might illuminate the capability of LES to predict visibility. Fig. 11 reveals that visibility follows the same general temporal developed ~~in all simulations~~ for all cases, with a rapid decrease ~~during~~ at fog formation, deepening, and dissipation; with minimum values around 100 m (which is ~~similar to the observations~~ close to the observed values). We also see noteworthy differences, particularly shortly before 0200 UTC (before fog deepening) at around 0545 UTC (shortly after sunrise). For both time marks, case ~~N1EXP~~ N1DIA - ~~N3EXP~~ N3DIA display sudden increases in visibility, due to an fast decrease of n_c in 2 m height; and which are not reproduced by case SAT, as n_c is fixed value in this case. The sudden increase in visibility around 0045 UTC in the observations is possibly related to this process. Also, the time marks of formation and dissipation vary. For cases ~~N1EXP~~ N1DIA - ~~N3EXP~~ N3DIA the formation time is significantly advanced compared to case SAT, while dissipation time only shows a small tendency towards earlier times, at least for ~~N1EXP and N3EXP. Case N2EXP~~ N1DIA and N3DIA. Case N2DIA displays a different behavior, with a later fog formation and higher visibility and accordingly earlier dissipation time. This is in line with the findings discussed above (i.e. a much weaker fog layer that, as a direct consequence, can dissipate much faster). Otherwise, all cases display almost identical visibility as soon as the fog has deepened.

Table 2. Table of fog's life cycle time marks.

Simulation	Onset	Maximum	Lifting	Dissipation
N1DIA	0025 UTC	0510 UTC	0810 UTC	1005 UTC
N2DIA	0050 UTC	0425 UTC	0755 UTC	0910 UTC
N3DIA	0025 UTC	0515 UTC	0810 UTC	0950 UTC

4.4.2 Time marks of the fog life cycle

The effect of the different droplet concentration (induced by the usage of different activation schemes) on the time marks of the fog life cycle is summarized in Tab. 2. While N1DIA and N3DIA have similar time marks, N2DIA stands out and show a delayed onset by 25 min, while the maximum liquid water mixing ratio is reached 45 min earlier than in the other cases.

5 Also lifting and dissipation are affected and occurred 15 min and 40 min (with respect to simulation N3DIA) earlier. This is due to a lesser absolute liquid water mixing ratio which evaporates faster by the incoming solar radiation. Therefore, it can be concluded that the use of different activation schemes (if they change the droplet number concentration) has an effect on the time marks on the life cycle as well as on the fog height and the amount of liquid water within the fog layer.

4.4.3 Budgets of liquid water and droplet number concentration

10 In this section we will analyze the budgets of liquid water and droplet number concentration in physical terms. As in the preceding section, we will use the cases with different activation parameterizations, since they provide us a range of different CCN concentrations. Figure 12a shows the profiles of the liquid water mixing ratio at 0400 UTC, 0600 UTC, and 0800 UTC, i.e at different times during the mature phase of the fog. A detailed analysis of budgets at other stages of the life cycle of the fog is beyond the scope of this paper. The maximum q_l in the fog layer is reached at approximately 0600 UTC at a height

15 of 60 m. Afterwards a further vertical growth of the fog can be observed, where no further increase in liquid water takes places as a result of larger vertical extent of the mixing layer and due to rising temperatures after sunrise(see Fig. ??a). Moreover, Fig. 12b,c show the liquid water budget during the mature phase of the fog at 0600 UTC, when the fog was fully developed. Almost all three cases show identical values for condensation rates (see Fig. 12b) in the lowest part of the fog layer, with values being in the same order as the evaporation rates, so that the net gain in this region appears to be small

20 (see Fig. 12b). However, the N2EXP N2DIA case (with the lowest n_c) exhibits a generally lower absolute evaporation rate compared to both other cases, which can be attributed to the slightly higher mean values of the relative humidity (not shown) than in N1EXP and N3EXPN1DIA and N3DIA. In the upper part of the fog layer, higher values of the condensation rate are observed (especially for N1EXP and N3EXPN1DIA and N3DIA) with a concurrent decrease in evaporation rates, leading to differently strong deepening of the fog layer. At a height of approximately 80 m a maximum of the evaporation rates can be

25 observed, representing the presence of subsaturated regions in this height and the top of the fog. Larger differences can be observed in the sedimentation rates: First and foremost the sedimentation is proportional to the liquid water mixing ratio (see

also Eq. 4). ~~However, the~~ The strength of sedimentation also depends on the mean radius of the droplets, which increases with decreasing number of activated drops. Here, a lower n_c for a given amount of liquid water leads to a higher mean radius, compared to a higher n_c where the same amount of water is distributed to more drops, decreasing the mean radius. Integrated over height all three cases exhibit approximately the same sedimentation rates. Therefore, case ~~N2EXP suffers the most from the~~ N2DIA experiences the strongest loss of liquid water due to sedimentation (in relative terms). Moreover, Fig. 12c shows that sedimentation partially counteracts the gains caused by condensation at the upper edge of the fog. ~~All in all it~~ The net advection transports liquid water from the second third of the fog layer (position of the maximum) to higher levels. It can be summarized that all ~~shown processes affect~~ terms contribute significantly to the net change of the liquid water mixing ratio~~.~~, illustrating that all microphysical processes deserve a proper modelling for radiation fog. In ~~However, in~~ the mature phase, ~~however,~~ sedimentation plays a key role, showing the highest values for the individual tendencies. As a result liquid water is slowly and constantly removed from the fog layer. These findings are in good agreement with previous investigations by Bott (1991).

The sum of all tendencies, which is shown in Fig. 12d, is the height-dependent change of the liquid water. Also here it can be seen that in the lower 50 m the net tendency is negative, while in higher levels we observe a positive tendency, so that the fog continues growing vertically, while the liquid water content within the fog layer decreases.

Figure 13a ~~shows~~ additionally shows the profiles of n_c ~~at 0400 UTC, 0600 UTC and 0800 UTC~~. We note that the profiles of the different cases differ quantitatively but not qualitatively. The stage of the fog can thus be identified in the profiles for all cases: At 0400 UTC highest supersaturations occur close to the ground due to cooling of the surface and near-surface air, leading to high activation rates and therefore high n_c near the surface (not shown). At 0600 UTC a well-mixed layer has developed that is driven by the radiative cooling from the fog top. While the turbulent mixing leads to a vertical well-mixed n_c, we note the maximum at the top, where the radiative cooling induces immense aerosol activation. This is ~~also displayed~~ further illustrated in the budget of the n_c ~~(see~~ in Fig. 13b,c~~), where the instantaneous rates for~~, where instantaneous data at 0600 UTC ~~are~~ is shown. Here, we see clearly that aerosol activation at the top of the fog layer is the dominant process in the mature phase of the fog, while activation near the surface is ~~relatively unimportant. Also, we see that both, advection and sedimentation are much less important than activation. Finally, we note that evaporation~~ comparably small. Evaporation of droplets, though small in magnitude, occurs only at the fog top, reflecting ~~updrafts~~ upward motions of foggy air penetrating the subsaturated air aloft where droplets then evaporate. Also, we see that both advection and sedimentation rates are much smaller than activation rates, so that the net change in n_c is controlled by the activation near the fog-top during the mature phase of the fog.

~~Table of fog's life cycle time marks. Simulation Onset Maximum Lifting DissipationN1EXP 0025 UTC 0510 UTC 0810 UTC 1005 UTC N2EXP 0050 UTC 0425 UTC 0755 UTC 0910 UTC N3EXP 0025 UTC 0515 UTC 0810 UTC 0950 UTC~~

~~The effect of the different activation schemes on the time of the fog life cycle is summarized in Tab. 2. While N1EXP and N3EXP have similar time marks, N2EXP stands out and show an delayed onset by 25 min, while the maximum liquid water mixing ratio is reached 45 min earlier, than in the other cases. Also lifting and dissipation are affected and occurred 15 min and 40 min (with respect to simulation N3EXP) earlier. This is due to a lesser absolute liquid water mixing ratio which evaporates~~
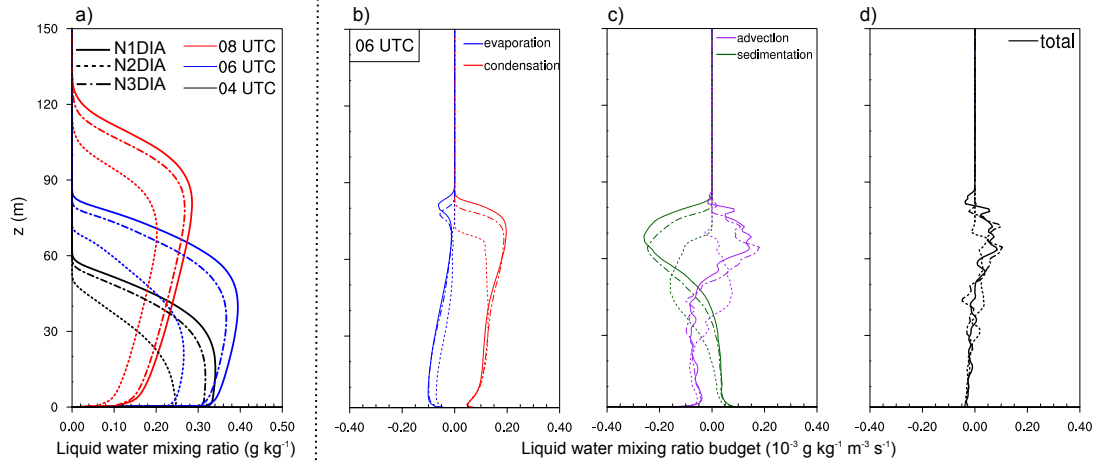
Figure 12. Profiles (instantaneously and horizontally averaged) of liquid water mixing ratio at 0400 UTC, 0600 UTC and 0800 UTC and profiles of ~~explicit~~ liquid water budget terms at 0600 UTC.
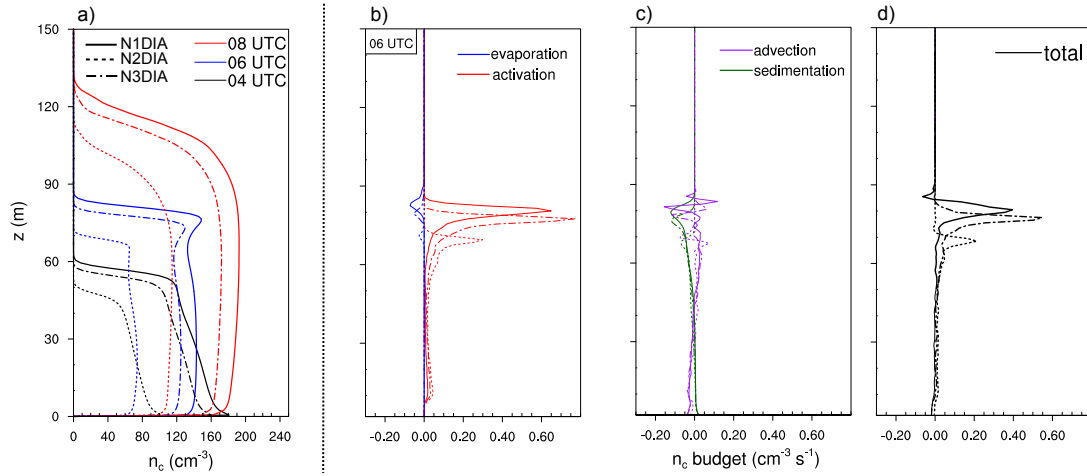

Figure 13. Profiles (instantaneously and horizontally averaged) of n_c at 0400 UTC, 0600 UTC and 0800 UTC and profiles of ~~explicit~~ n_c budget terms at 0600 UTC.

~~faster by the incoming solar radiation. Therefore, it can be concluded that the use of different activation schemes (if they change the droplet number concentration) has an effect on the time marks~~

5   Conclusions

24

The main objective of this work was to investigate the influence of the choice of the supersaturation calculation and activation parameterizations used in LES models on the life cycle ~~as well as on the fog height and the amount of liquid water within the fog layer.~~

5.1 ~~Impact of supersaturation calculation on CCN activation~~

5 of simulated nocturnal deep radiation fog under typical continental aerosol conditions. For this purpose we performed a series of LES runs based on a typical deep fog event as observed at Cabauw (Netherlands).

~~The impact of different methods modelling supersaturation on the CCN activation for a radiation fog event is investigated following Lebo et al. (e.g. 2012); Thouron et al. (e.g. 2012). Figure 6 shows the LWP for simulations applying the activation scheme~~ In the main part of this study we applied a two-moment microphysics scheme with an activation parameterization

10 of Cohard et al. (1998) and ~~using saturation adjustment (N2SAT), the explicit scheme (N2EXP)~~ investigated the influence of three different (but commonly used) supersaturation calculation methods, i.e. saturation adjustment, a diagnostic method, and a prognostic ~~scheme (N2PRG) for calculating supersaturations. It can be seen that the prognostic approach and explicit methods produces very similar values for the LWP . However,~~ method, on the life cycle and LWP of the simulated fog event. From the results we found that in case of saturation adjustment ~~the LWP is nearly 70% higher than for the other schemes. In Fig. 7~~

15 ~~profiles of the liquid water mixing ratio (left) and~~ nearly 60% higher droplet number concentration ~~(right) are shown. Here, the number concentration in case N2EXP exhibits slightly higher values as N2PRG, but are both at approximately 100 cm^{-3} at 0600 UTC. In contrast, in simulation N2SAT a number concentration of 150 cm^{-3} is observed. Those differences are explained by the different methods for calculating the supersaturation, since activation is the main process altering the droplet number concentration (all other terms of Eq. 3 are less important as shown in Fig. 13). Due to that one can implicitly derive from the~~

20 ~~droplet number concentration that the prognosed and diagnosed values for the supersaturation using the explicit method and the prognostic method are quite similar. As saturation adjustment removes all supersaturation during one time step, a method for approximating the supersaturation is used (see Eq. 15). By that, the case N2SAT produces a droplet number concentration of 150 cm^{-3} at 0600 UTC, which is about 50% higher in comparision to N2EXP and N2PRG. However, these differences between N2SAT and N2EXP/N2PRG are in good agreement with the found values of Thouron et al. (2012) for a stratocumulus case~~

25 ~~(see their Fig. 2) where the number concentration of the explicit and prognostic method were also quite similar and the case with saturation adjustment overestimates the supersaturation and therefore the droplet number concentration. As outlined in the section before, the number concentration has a crucial impact on the LWP as well as on the times~~ are produced in comparison to simulation with the diagnostic or prognostic method. This results in a more than 70% higher LWP for the saturation adjustment case and a later occurrence of lifting and dissipation of the fog ~~. Time series of LWP for simulations using saturation adjustment~~

30 ~~(N2SAT, black), the explicit scheme (N2EXP, blue) and the prognostic method (N2PRG, red). All cases uses the activation scheme of Cohard et al. (1998).~~

~~Profiles for liquid water mixing ratio and droplet number concentration at 0400 UTC, 0600 UTC and 0800 UTC.~~

5.0.1 ~~Grid spacing sensitivity study~~

~~As Fig. 6 but also 2 m (dot-dashed) and 4 m (dashed).~~

~~To evaluate the effect of grid spacing with different methods for calculating the supersaturation on CCN activation we repeated cases N2SAT, N2EXP and N2PRG each with two coarser grid spacings of 2 m and 4 m. The general effect of the grid spacing to the temporal development and structure of radiation fog is discussed in detail in Maronga and Bosveld (2017). In this section, we will thus focus only on relative changes in LWP due to different microphysical parameterizations at different spatial model resolution. In Fig.8 the LWP for the different supersaturation calculations and grid spacing is shown.~~

~~We note, that for all grid spacings the the major difference persists between the case using saturation adjustment, which produces a maximum value of approximately 30 g m^{-2} for the LWP in comparision to the explicit and prognostic method which both exhibit a maximum of approximately 20 g m^{-2}. However, interestingly,~~ layer. An explanation for such differences between the schemes can be found in the general assumptions made within the methods. As saturation adjustment assumes that the complete water vapor surplus is removed within one time step, the ~~relative differences (ratio of N2EXP to N2PRG) in the LWP between the explicit and prognostic methods increases as the grid spacing gets larger. Quantitatively speaking, in case of 1 m grid spacing~~ supersaturation used for activation must be parameterized. In agreement with Thouron et al. (2012) we found that those values are higher as in the other cases, which leads to great feedback of the fog layer. Moreover, we found that the diagnostic method and ~~the relative difference of the LWP is 2.1% between N2EXP and N2PRG during the mature phase while for the case with a grid spacing of 4 m it reaches 8.1%. This increase of the relative changes might be explained by the fact that the explicit scheme is very sensitive to small errors (e.g. induced by the numerical advection) in the fields of T and q_v (e.g. Morrison and Grabowski, 2008; Thouron et al., 2012). A coarser spatial resolution favors that the error introduced by spurious supersaturation gets larger. Due to that we suppose that the increased differences (see Fig. 8) by larger grid spacings are induced by spurious supersaturation, which affect the CCN activation and by that infuence the LWP of~~ prognostic method yield similar results. However, in a grid spacing sensitivity study we observed that the relative differences between the ~~fog layer. As sedimentation and~~ prognostic and diagnostic approach increase as the spatial resolution decrease. We assume that this is due to larger errors of spurious supersaturations which lead to an overestimation of activation in the diagnostic case. This in turn effect the sedimentation velocity as well as the effective radius and hence the ~~radiative cooling, which are key processes for fog, are sensitive to the number of activated droplets such errors should be considered~~ results in higher values for the LWP.

~~The main objective of this work was to investigate the influence of the choice of the microphysical parameterization used in LES models on the life cycle of simulated nocturnal deep radiation fog under typical continental aerosol conditions. For this purpose we performed a series of LES runs for a typical fog event observed at Cabauw (Netherlands). First~~ In a further test, using a one-moment microphysics scheme, we compared the possible error introduced ~~when~~ by using saturation adjustment in comparison with an ~~explicit~~ diagnostic and prognostic method for calculating the supersaturation for diffusional growth~~. The~~, i.e. neglecting activation and prescribing a constant droplet number concentration. With this assumptions we were able to isolate the error introduced by saturation adjustment on condensation and evaporation. However, the results showed that, although the model time step was inappropriate for the assumptions made during saturation adjustment, the differences in LWP

are at most 1% and the general life cycle is not affected. This could be attributed to the fact that the typical supersaturations in fog are in the range of a few tenths of a percent, and the resulting absolute differences are too small to induce a further influence on dynamics, microphysics or radiation. This result implies that saturation adjustment is an acceptable method if no activation parameterization is available (with simultaneous consideration that the latter is highly recommended).

5   In a second part of our study, the effect of different activation schemes of Twomey (1959), Cohard et al. (1998) and Khvorostyanov and Curry (2006) on the simulated fog life cycle ~~were investigated(cases N1EXP to N3EXP)~~was investigated. Even though these parameterizations ~~are very~~appear to be rather similar, our results indicate that the resulting number of activated aerosols (and consequently the number of droplets), known to be a crucial parameter for the fog development, ~~differed significantly. An analysis of the budgets of~~can differ significantly. However, it must be mentioned that these differences are

10   attributed to the fact that the CCN concentration is different for the investigated schemes. This part of the study can thus also be understood as a sensitivity study for different CCN concentrations realized by the usage of different activation schemes.

In order to get a deeper insight into the spatial and temporal development of deep radiation fog, we performed an additional analysis of budgets n_c and q_l ~~showed that diffusional growth is the major process for generating liquid water, but was found to be independent of the number of droplets and thus comparable in magnitude in all cases. In contrast, the sedimentation~~

15   ~~rates showed a different behaviour: On the one hand, these were found to be proportional to~~during the mature phase of the ~~liquid water mixing ratio, which is high in cases N1EXP and N3EXP. On the other hand, the sedimentation depends on the mean radius of the droplets, which is higher in the case of fewer activated aerosols (case N2EXP). Overall, this leads to almost identical absolute integral sedimentation rate for the three schemes. However, this means that~~fog for simulations with different aerosol activation parameterizations. We found that gain of liquid water is ~~removed by sedimentation more rigorously~~

20   ~~in case N2 (in relative terms) compared to cases N1EXP and N3EXP. Moreover, we could show that most aerosol activation happens near the surface during the formation phase of the fog , while the maximum number of activated aerosols during the mature phase is located~~dominated by condensational growth throughout the fog layer with a maximum at the top of the fog layer ~~. The latter results from the radiative coolingof the fog top, producing the largest supersaturations. Nevertheless, this radiative cooling, triggers a top-down convective layer, so that the~~(due to longwave radiative cooling) and by significant

25   sedimentation of fog droplets from upper levels towards lower levels, while only little liquid water is lost by sedimentation (to the ground) and evaporation. The fact that the simulated cases displays significant differences in the fog strength could be traced back to the ~~droplets are well mixed, leading to an evenly distributed number concentration throughout the fog layer. As the sedimentation process and radiative cooling are proportional to the droplet number concentration, case N2EXP shows that the LWP is significantly reduced as a result of smaller droplet number concentrations. Moreover,~~differences in the condensational

30   growth at the fog top, induced by different activation of CCN. For n_c, our simulations indeed indicate that activation is the dominant process, located in a narrow height level, while all other processes (i.e. evaporation, advection, and sedimentation) were found to be comparably small. The amount of generated liquid water thus is a direct consequence of the ~~time marks of the fog life cycle are also affected: If the fog layer contains a smaller amount of liquid water, lifting and dissipation occur earlier, because less energy is required for evaporation of a thinner fog layer.~~

~~At last we investigated the impact of different (commonly used) supersaturation calculations on CCN activation by employing a single activation scheme but using the aforementioned different scheme considering supersaturation. From this study we found that in case of saturation adjustment higher droplet number concentration are produced. The explicit method and the prognostic method instead performed quite similar. However, in a grid spacing sensitivity study we observed that the relative differences between the prognostic and explicit approach increase as the spatial resolution decrease. We assume that this is due to larger errors of spurious supersaturations which lead to higher droplet concentrations and thus also effect the LWP~~ strength of the activation process and is thus related to the number of CCN and accordingly the activation parameterization used in the model.

In summary, the present study indicates that the choice of the used ~~microphysics parameterization~~ supersaturation calculation can be a key factor for the simulation of radiation fog. ~~While the effect of applying saturation adjustment in case of assuming a constant droplet number concentration on the diffusional growth is negligible,~~ In agreement with Thouron et al. (2012) we recommend to use the prognostic approach to calculate the ~~supersaturations~~ supersaturation for fog layer in case of a ~~full~~ two-moment microphysics considering activation. ~~Moreover~~Therewith, the effect of spurious cloud edge supersaturation is mitigated and too large activation rates are omitted. Further, the choice of the chosen activation scheme has ~~an noticeable impact of~~ a noticeable impact on the number concentration of CCN and hence on the LWP and fog ~~height~~layer depth. However, we have no means to give advice which activation parameterization performs best. In order to give a more educated recommendation here, we would need observational data of size distributions from aerosol and fog droplets.

In order to overcome ~~these~~ the remaining limitations of the present study ~~, we plan to revisit~~ that are related to microphysical parameterizations, we are currently working on a follow-up study in which we are revisiting this particular fog case using a Lagrangian particle-based approach to simulate the microphysics of droplets~~which~~. This will allow for explicitly simulating the development of the 3D droplet size distribution in the fog layer (e.g. Shima et al., 2009). This approach will also allow to resolve all relevant microphysical processes such as activation and diffusional growth directly, instead of parameterizing them. As such simulations are computationally very expensive, only a very limited number of simulations are feasible at the moment, so that most future numerical investigations will - as in the present work - rely on bulk microphysics parameterizations. Based on the results using the Lagrangian approach, however, we hope to be able to give an educated recommendation on the best choice for such bulk parameterizations.

6 ~~**Activation spectrum**~~

~~In Fig. 2 the activation spectrum for the three different activation schemes of Twomey (1959) (N1EXP), Cohard et al. (1998) (N2EXP) and Khvorostyanov and Curry (2006) (N3EXP) are shown. Activation spectrum for three different activation schemes of Twomey (1959)(N1EXP), Cohard et al. (1998)(N2EXP) and Khvorostyanov and Curry (2006)(N3EXP).~~

References

Abdul-Razzak, H. and Ghan, S. J.: A parameterization of aerosol activation: 2. Multiple aerosol types, J. Geophys. Res. Atmos., 105, 6837–6844, 2000.

Ackerman, A. S., VanZanten, M. C., Stevens, B., Savic-Jovcic, V., Bretherton, C. S., Chlond, A., Golaz, J.-C., Jiang, H., Khairoutdinov, M., Krueger, S. K., et al.: Large-eddy simulations of a drizzling, stratocumulus-topped marine boundary layer, Mon. Weather Rev., 137, 1083–1110, 2009.

Árnason, G. and Brown Jr, P. S.: Growth of cloud droplets by condensation: A problem in computational stability, J. Atmos. Sci., 28, 72–77, 1971.

Beare, R. J., Macvean, M. K., Holtslag, A. A., Cuxart, J., Esau, I., Golaz, J.-C., Jimenez, M. A., Khairoutdinov, M., Kosovic, B., Lewellen, D., et al.: An intercomparison of large-eddy simulations of the stable boundary layer, Boundary-Layer Meteorol., 118, 247–272, 2006.

Bergot, T.: Small-scale structure of radiation fog: a large-eddy simulation study, Quart. J. Roy. Meteor. Soc., 139, 1099–1112, 2013.

Boers, R., Baltink, H. K., Hemink, H., Bosveld, F., and Moerman, M.: Ground-based observations and modeling of the visibility and radar reflectivity in a radiation fog layer, J. Atmos. Ocean Technol., 30, 288–300, 2013.

Bott, A.: On the influence of the physico-chemical properties of aerosols on the life cycle of radiation fogs, Boundary-Layer Meteorol., 56, 1–31, 1991.

Bott, A. and Trautmann, T.: PAFOG—a new efficient forecast model of radiation fog and low-level stratiform clouds, Atmos. Res., 64, 191–203, 2002.

Bougeault, P.: Modeling the trade-wind cumulus boundary layer. Part I: Testing the ensemble cloud relations against numerical data, J. Atmos. Sci., 38, 2414–2428, 1981.

Boutle, I., Price, J., Kudzotsa, I., Kokkola, H., and Romakkaniemi, S.: Aerosol-fog interaction and the transition to well-mixed radiation fog, Atmos. Chem. Phys., 18, 7827–7840, 2018.

Clark, T. L.: Numerical modeling of the dynamics and microphysics of warm cumulus convection, J. Atmos. Sci., 30, 857–878, 1973.

Clough, S. A., Shephard, M. W., Mlawer, E. J., Delamere, J. S., Iacono, M. J., Cady-Pereira, K., Boukabara, S., and Brown, P. D.: Atmospheric radiative transfer modeling: A summary of the AER codes, Short Communication, J. Quant. Spectrosc. Radiat. Transfer, 91, 233–244, 2005.

Cohard, J.-M. and Pinty, J.-P.: A comprehensive two-moment warm microphysical bulk scheme. I: Description and tests, Quart. J. Roy. Meteor. Soc., 126, 1815–1842, 2000.

Cohard, J.-M., Pinty, J.-P., and Bedos, C.: Extending Twomey's analytical estimate of nucleated cloud droplet concentrations from CCN spectra, J. Atmos. Sci., 55, 3348–3357, 1998.

Cohard, J.-M., Pinty, J.-P., and Suhre, K.: On the parameterization of activation spectra from cloud condensation nuclei microphysical properties, J. Geophys. Res. Atmos., 105, 11 753–11 766, 2000.

Deardorff, J. W.: Stratocumulus-capped mixed layers derived from a three-dimensional model, Boundary-Layer Meteorol., 18, 495–527, 1980.

Geoffroy, O., Brenguier, J.-L., and Sandu, I.: Relationship between drizzle rate, liquid water path and droplet concentration at the scale of a stratocumulus cloud system, Atmos. Chem. Phys., 8, 4641–4654, 2008.

Geoffroy, O., Brenguier, J.-L., and Burnet, F.: Parametric representation of the cloud droplet spectra for LES warm bulk microphysical schemes, Atmos. Chem. Phys., 10, 4835–4848, 2010.

Grabowski, W. W. and Morrison, H.: Toward the mitigation of spurious cloud-edge supersaturation in cloud models, Mon. Weather Rev., 136, 1224–1234, 2008.

Gultepe, I., Müller, M. D., and Boybeyi, Z.: A new visibility parameterization for warm-fog applications in numerical weather prediction models, J. Appl. Meteor. Climatol., 45, 1469–1480, 2006.

Gultepe, I., Tardif, R., Michaelides, S., Cermak, J., Bott, A., Bendix, J., Müller, M. D., Pagowski, M., Hansen, B., Ellrod, G., et al.: Fog research: A review of past achievements and future perspectives, in: Fog and Boundary Layer Clouds: Fog Visibility and Forecasting, pp. 1121–1159, Springer, 2007.

Gultepe, I., Hansen, B., Cober, S., Pearson, G., Milbrandt, J., Platnick, S., Taylor, P., Gordon, M., and Oakley, J.: The fog remote sensing and modeling field project, Bull. Amer. Meteor. Soc., 90, 341–359, 2009.

Haeffelin, M., Bergot, T., Elias, T., Tardif, R., Carrer, D., Chazette, P., Colomb, M., Drobinski, P., Dupont, E., Dupont, J.-C., et al.: PARIS-FOG: shedding new light on fog physical processes, Bull. Amer. Meteor. Soc., 91, 767–783, 2010.

Hammer, E., Gysel, M., Roberts, G., Elias, T., Hofer, J., Hoyle, C., Bukowiecki, N., Dupont, J.-C., Burnet, F., Baltensperger, U., et al.: Size-dependent particle activation properties in fog during the ParisFog 2012/13 field campaign, Atmos. Chem. Phys., 14, 10 517–10 533, 2014.

Heus, T., Van Heerwaarden, C., Jonker, H. J., Siebesma, A. P., Axelsen, S., Van Den Dries, K., Geoffroy, O., Moene, A., Pino, D., De Roode, S., et al.: Formulation of the Dutch Atmospheric Large-Eddy Simulation (DALES) and overview of its applications, Geosci. Model Dev., 3, 415, 2010.

Khairoutdinov, M. and Kogan, Y.: A new cloud physics parameterization in a large-eddy simulation model of marine stratocumulus, Mon. Weather Rev., 128, 229–243, 2000.

Khvorostyanov, V. I. and Curry, J. A.: Aerosol size spectra and CCN activity spectra: Reconciling the lognormal, algebraic, and power laws, J. Geophys. Res. Atmos., 111, 2006.

Kokkola, H., Korhonen, H., Lehtinen, K., Makkonen, R., Asmi, A., Järvenoja, S., Anttila, T., Partanen, A.-I., Kulmala, M., Järvinen, H., et al.: SALSA–a Sectional Aerosol module for Large Scale Applications, Atmos. Chem. Phys., 8, 2469–2483, 2008.

Lac, C., Chaboureau, J.-P., Masson, V., Pinty, J.-P., Tulet, P., Escobar, J., Leriche, M., Barthe, C., Aouizerats, B., Augros, C., Aumond, P., Auguste, F., Bechtold, P., Berthet, S., Bielli, S., Bosseur, F., Caumont, O., Cohard, J.-M., Colin, J., Couvreux, F., Cuxart, J., Delautier, G., Dauhut, T., Ducrocq, V., Filippi, J.-B., Gazen, D., Geoffroy, O., Gheusi, F., Honnert, R., Lafore, J.-P., Lebeaupin Brossier, C., Libois, Q., Lunet, T., Mari, C., Maric, T., Mascart, P., Mogé, M., Molinié, G., Nuissier, O., Pantillon, F., Peyrillé, P., Pergaud, J., Perraud, E., Pianezze, J., Redelsperger, J.-L., Ricard, D., Richard, E., Riette, S., Rodier, Q., Schoetter, R., Seyfried, L., Stein, J., Suhre, K., Taufour, M., Thouron, O., Turner, S., Verrelle, A., Vié, B., Visentin, F., Vionnet, V., and Wautelet, P.: Overview of the Meso-NH model version 5.4 and its applications, Geosci. Model Dev., 11, 1929–1969, https://doi.org/10.5194/gmd-11-1929-2018, https://www.geosci-model-dev.net/11/1929/2018/, 2018.

Lebo, Z. J., Morrison, H., and Seinfeld, J. H.: Are simulated aerosol-induced effects on deep convective clouds strongly dependent on saturation adjustment?, Atmos. Chem. Phys., 12, 9941–9964, https://doi.org/10.5194/acp-12-9941-2012, 2012.

Maalick, Z., Kühn, T., Korhonen, H., Kokkola, H., Laaksonen, A., and Romakkaniemi, S.: Effect of aerosol concentration and absorbing aerosol on the radiation fog life cycle, Atmos. Environ., 133, 26–33, 2016.

Maronga, B. and Bosveld, F.: Key parameters for the life cycle of nocturnal radiation fog: a comprehensive large-eddy simulation study, Quart. J. Roy. Meteor. Soc., 2017.

Maronga, B., Gryschka, M., Heinze, R., Hoffmann, F., Kanani-Sühring, F., Keck, M., Ketelsen, K., Letzel, M. O., Sühring, M., and Raasch, S.: The Parallelized Large-Eddy Simulation Model (PALM) version 4.0 for atmospheric and oceanic flows: model formulation, recent developments, and future perspectives, Geosci. Model Dev., 2015.

Mazoyer, M., Lac, C., Thouron, O., Bergot, T., Masson, V., and Musson-Genon, L.: Large eddy simulation of radiation fog: impact of dynamics on the fog life cycle, Atmos. Chem. Phys., 17, 13 017, 2017.

Mazoyer, M., Burnet, F., Denjean, C., Roberts, G. C., Haeffelin, M., Dupont, J.-C., and Elias, T.: Experimental study of the aerosol impact on fog microphysics, Atmospheric Chemistry and Physics, 19, 4323–4344, https://doi.org/10.5194/acp-19-4323-2019, https://www.atmos-chem-phys.net/19/4323/2019/, 2019.

Mensah, A., Holzinger, R., Otjes, R., Trimborn, A., Mentel, T. F., Brink, H. t., Henzing, B., and Kiendler-Scharr, A.: Aerosol chemical composition at Cabauw, The Netherlands as observed in two intensive periods in May 2008 and March 2009, Atmos. Chem. Phys., 12, 4723–4742, 2012.

Morrison, H. and Grabowski, W. W.: Comparison of bulk and bin warm-rain microphysics models using a kinematic framework, J. Atmos. Sci., 64, 2839–2861, 2007.

Morrison, H. and Grabowski, W. W.: Modeling supersaturation and subgrid-scale mixing with two-moment bulk warm microphysics, J. Atmos. Sci., 65, 792–812, 2008.

Nakanishi, M.: Large-eddy simulation of radiation fog, Boundary-Layer Meteorol., 94, 461–493, 2000.

Pruppacher, H. R. and Klett, J. D.: Microphysics of clouds and precipitation, Kluwer Academic Publishers, Dordrecht, Netherlands, 2nd revised edn., 1997.

Seifert, A. and Beheng, K. D.: A double-moment parameterization for simulating autoconversion, accretion and selfcollection, Atmos. Res., 59, 265–281, 2001.

Seifert, A., Khain, A., Pokrovsky, A., and Beheng, K. D.: A comparison of spectral bin and two-moment bulk mixed-phase cloud microphysics, Atmos. Res., 80, 46–66, 2006.

Shima, S., Kusano, K., Kawano, A., Sugiyama, T., and Kawahara, S.: The super-droplet method for the numerical simulation of clouds and precipitation: A particle-based and probabilistic microphysics model coupled with a non-hydrostatic model, Quart. J. Roy. Meteor. Soc., 135, 1307–1320, 2009.

Stolaki, S., Haeffelin, M., Lac, C., Dupont, J.-C., Elias, T., and Masson, V.: Influence of aerosols on the life cycle of a radiation fog event. A numerical and observational study, Atmos. Res., 151, 146–161, 2015.

Thouron, O., Brenguier, J.-L., and Burnet, F.: Supersaturation calculation in large eddy simulation models for prediction of the droplet number concentration, Geosci. Model Dev., 5, 761–772, 2012.

Twomey, S.: The nuclei of natural cloud formation part II: The supersaturation in natural clouds and the variation of cloud droplet concentration, Pure Appl. Geophys., 43, 243–249, 1959.

Wicker, L. J. and Skamarock, W. C.: Time-splitting methods for elastic models using forward time schemes, Mon. Weather Rev., 130, 2088–2097, 2002.

Williamson, J.: Low-storage runge-kutta schemes, J. Comput. Phys., 35, 48–56, 1980.

Zhang, X., Musson-Genon, L., Dupont, E., Milliez, M., and Carissimo, B.: On the influence of a simple microphysics parametrization on radiation fog modelling: A case study during parisfog, Boundary-Layer Meteorol., 151, 293–315, 2014.